Chapter 4

MICROBIAL DIVERSITY AND IRON OXIDATION AT OKUOKU-HACHIKUROU ONSEN, A JAPANESE HOT SPRING ANALOG OF PRECAMBRIAN IRON FORMATION

Ward, LM, A Idei, S Terajima, T Kakegawa, WW Fischer, and SE McGlynn. Microbial diversity and iron oxidation at Okuoku-hachikurou Onsen, a Japanese hot spring analog of Precambrian iron formation. Geobiology, in revision.

Abstract:

Banded Iron Formations (BIFs) are rock deposits common in the Archean and Paleoproterozoic (and regionally Neoproterozoic) sedimentary successions. Multiple hypotheses for their deposition exist, principally invoking the precipitation of iron via the metabolic activities of oxygenic, photoferrotrophic, and/or aerobic iron-oxidizing bacteria. Some isolated environments support chemistry and mineralogy analogous to processes involved in BIF deposition, and their study can aid in untangling the factors that lead to iron precipitation. One such process analog system occurs at Okuoku-hachikurou (OHK) Onsen in Akita Prefecture, Japan. OHK is an iron- and CO2-rich, circumneutral hot spring that produces a range of precipitated mineral textures containing fine laminae of aragonite and iron oxides that resemble BIF fabrics. Here, we have performed metagenomic 16S amplicon sequencing of microbial communities across the range of microenvironments in OHK to describe the microbial diversity present and to gain insight into the cycling of iron, oxygen, and carbon in this ecosystem. These analyses suggest that productivity at OHK is based on aerobic iron-oxidizing Gallionellaceae. In contrast to other BIF analog sites,

Cyanobacteria, anoxygenic phototrophs, and iron-reducing microorganisms are present at only low abundances. These observations support a hypothesis where low growth yields and high stoichiometry of iron oxidized per carbon fixed by aerobic iron-oxidizing chemoautotrophs like Gallionellaceae, result in accumulation of iron oxide phases without stoichiometric buildup of organic matter; this system supports little dissimilatory iron reduction, further setting OHK apart from other process analog sites where iron oxidation is primarily driven by phototrophic organisms. This positions OHK as a study area where the controls on primary productivity in iron-rich environments can be elucidated. When compared with geological data, the metabolisms and mineralogy at OHK are most similar to specific BIF occurrences deposited after the Great Oxygenation Event, and generally discordant with those that accumulated before it.

Background:

Banded Iron Formation (BIF) is a characteristic lithotype in many Precambrian basins. These finely laminated, iron-rich (>15% Fe by weight) sedimentary deposits are not only economically critical sources of iron ore (particularly after post-depositional weathering and hydrothermal processes oxidize, leach, and upgrade the ore, Morris 1980, Beukes 1984), but may provide a record of biological activity on the early Earth (e.g. Harder 1919, Konhauser et al. 2002, Kappler et al. 2005).

Despite their prevalence in the early rock record, the processes by which BIFs are deposited are not well understood. It is generally hypothesized that BIFs formed as a result of transport and concentration of ferrous iron (as $Fe^{2+}_{(aq)}$) in seawater under anoxic and sulfur-poor conditions, followed by oxidation and precipitation of iron as ferric iron phases

(Holland 1973, Drever 1974, Holland 1984). However, it is important to note that the primary mineralogy that made up the precursor sediments to BIF remains uncertain in many cases, and the significance of iron oxidation during BIF deposition remains an area of active debate (Konhauser et al. 2002, Kappler et al. 2004, Kappler et al. 2005, Bekker et al. 2013, Posth et al. 2013, Rasmussen et al. 2013, Rasmussen et al. 2015, Rasmussen et al. 2016, Tosca et al. 2016). Different hypotheses for BIF deposition invoke a range of iron oxidation processes, including abiotic iron oxidation by UV light (e.g. Cairns-Smith 1978, Francois 1986), indirectly biologically by O_2 sourced from oxygenic photosynthesis by Cyanobacteria (e.g. Cloud 1973), or directly biologically by aerobic iron-oxidizing bacteria (e.g. Chan et al. 2016) or by anaerobic iron-oxidizing phototrophic bacteria (e.g. Widdel et al. 1993, Kappler et al. 2005). BIFs do not form in marine sedimentary basins today due to the O_2 and sulfate content of seawater (Canfield 1998), which prevents the mobilization and concentration of sufficient amounts of dissolved iron in seawater and shallow pore fluids (Holland 1973). However, a range of potential analog environments can be observed today that may reveal key processes associated with the deposition of BIFs. These include permanently stratified lakes, such as Lake Matano in Indonesia (Crowe et al. 2008), and iron-rich hot springs, such as Chocolate Pots in Yellowstone National Park (Pierson et al. 1999). These systems contain anoxic, iron-rich waters that produce iron oxides and other Fe-bearing phases through a range of processes. In Lake Matano, iron oxide production is thought to be driven largely by photoferrotrophy (Crowe et al. 2008), while at Chocolate Pots hot spring iron oxidation is driven primarily by abiotic reaction of iron with O_2 produced by Cyanobacteria (Pierson et al. 1999, Pierson and Parenteau 2000, Trouwborst

et al. 2007). Terrestrial hot springs can provide unique environments in which high concentrations of dissolved iron can exist at circumneutral conditions due to rock weathering by anoxic source waters; they also provide access to novel microbial diversity which is rare or absent from typical surface environments. While these hot spring fluids are not perfect compositional mimics of Precambrian seawater, the geomicrobiological processes they support and the resulting facies and fabrics can provide process analogs for understanding depositional mechanics of at least some BIFs. This is particularly useful for evaluating the relative roles that different microbiological processes (e.g. photoferrotrophy, aerobic iron oxidation, and oxygenic photosynthesis) may have played in the deposition of different BIF facies. A crucial but understudied aspect of BIF deposition in modern analog environments is the relative delivery fluxes of iron oxides and organic carbon to sediments, and the average oxidation state of the resultant iron formations; trends in the proportion of ferrous to ferric iron in ancient BIFs have long been observed in the rock record (e.g. Klein 2005)—and these can reflect the redox state of the environment at the time of deposition, as well as the particular physiologies and metabolisms responsible for iron oxidation (Fischer and Knoll 2009)(Supplemental Information). Though it has been little exploited, the metabolic yield and efficiency of the microbial metabolisms driving iron oxidation will be a factor in the mineralogy and redox chemistry of diagenetically stabilized iron formation lithologies. Currently, knowledge of the microbial metabolisms and processes that lead to different mineral assemblages (and ferric:ferrous ratios) in modern environments remains meager. Characterization of the microbial communities in the context of the organic carbon content and redox state of iron in the solids accumulating in BIF analogs deposited

differentially by photoferrotrophs, Cyanobacteria, and aerobic iron oxidizers will help to connect observations of ancient BIFs to the geobiological processes responsible for iron oxide deposition

In this study, we investigated a novel BIF-analog environment at Okuoku-hachikurou Onsen (OHK) in Akita Prefecture, Japan. OHK is an iron- and carbonate-rich, circumneutral hot spring with anoxic source waters, which produces extensive iron oxide and aragonite travertine with mineralogical and textural features resembling BIF (Takashima et al. 2011). To study the microbial diversity of OHK and evaluate the potential roles of different microbial metabolisms in producing mineral deposits at OHK, we collected mineral precipitates and filtered spring water from points along the outflow of the stream for analysis using microscopy and characterization of the microbial community via metagenomic 16S amplicon sequencing. These data reveal that productivity and iron oxidation at OHK is primarily driven by aerobic, iron-oxidizing taxa related to the genus *Sideroxydans*, and consequently the environment produces sediments that are organic-lean and contain a high proportion of ferric iron phases—an early diagenetic precondition to the highly oxidized BIF facies deposited in certain environments after the Great Oxygenation Event.

Materials and Methods:

Geological context and sedimentology of OHK:

OHK is located in Akita Prefecture, Japan, at 40.407925N, 140.754744E (Figure 1), in an active region of the Tohoku volcanic arc, generated by the subduction of the Pacific Plate; the local bedrock geology consists of Miocene–Holocene green tuff and

felsic volcanic rocks (Shimazu et al. 1965). OHK consists of a single subsurface water source that originates from a mining exploration borehole drilled in the 1960s. This borehole emerges into a 2 m diameter source pool, with a submerged shelf around the edge of the borehole at 1.2 m depth. At the time of our study in November 2015, water emerged from the borehole at 44.3°C, high in Fe(II), very low in oxygen (Table 1), and displayed continuous and vigorous ebullition of CO_2 (Figure 2). The source pool contains abundant suspended fine flocs of hydrous iron oxides. The early crystalline iron oxides phases at OHK consist of ferrihydrite (Takashima et al. 2011), though this may age into more ordered iron oxide minerals such as hematite, goethite, or lepidocrosite in travertines. From the source pool to the rotenburo (Figure 2), the stream flows over a mineralized substrate comprised of well-lithified, finely laminated aragonite and iron oxide travertine with a smooth texture and mottled coloration ranging from white aragonite to orange and red iron oxides (Figure 2). Surfaces of pools, channels, and canals are coated in fine, orange colored iron oxide flocs. Mature iron oxide phases within travertine appear dark red. Travertine accumulates around pool edges as lobate walls ~10 cm in width. Where spring water overflows the edges of pools travertine terraces develop with a characteristic ~5 cm step size and up to about a half meter in total height. These terraces superficially resemble those found in both circumneutral- and acidic-iron-rich systems elsewhere (e.g. Yellowstone National Park, Fouke 2011, and the Tintillo River, Spain, España et al. 2007); the occurrence of similar large scale morphologies across very geochemically different environments suggests that hydrology—as much as geochemistry or microbial processes—plays a role in the travertine morphologies (Fouke 2011).

An old outflow channel emerges from the source pool, but was largely inactive at the time of our sampling; flow into this channel has been blocked and redirected through canals to the rotenburo. This channel is ~5 cm deep, partially mixes with the source pool due to swashing caused by CO_2 ebullition, but is otherwise stagnant. Thin plates of aragonite (<1 mm) coat the water surface of the channel, and in some areas thin microbial biofilms have developed on the bottom of the channel.

Water emerging from the source pool predominantly flows through shallow (5-10 cm) canals into a ~1 m diameter pool used for bathing (rotenburo). Rock surfaces in the canals and rotenburo are coated in iron oxide flocs. Water flows out from the rotenburo through additional shallow canals and ultimately develops into a sheeted flow on the hill slope, where continual degassing of CO_2 leads to formation of bubbles. Many bubbles become encrusted with aragonite and mineralized (Figure 2).

While no substantial accumulation of microbial biomass is visible within the source pool, rotenburo, or canals, thin (<1 mm) patchy green biofilms occur along the rim of the source pool and old stream (Figure 2). These were sampled for the Shallow Source and Old Stream Mineral samples.

Downstream, OHK preserves unique mineralized bubbles. As CO_2 degasses from the spring water, dissolved inorganic carbon concentrations drop and the carbonate saturation state increases, prompting aragonite precipitation. This occurs sufficiently quickly in OHK that bubbles develop coatings of aragonite and are mineralized *in situ*. These bubbles encrust and provide a possible preservation mechanism for a wide range of organic materials, including leaves, arthropods, and biofilms in this section of the spring.

Preservation of organic structures by iron minerals has been observed previously in acidic iron-rich environments at Rio Tinto, Spain, where fossil structures endure for millions of years (Fernandez-Remolar and Knoll 2008). The rapid mineralization of iron oxides and aragonite at OHK may therefore also serve as a mechanism for preserving key biological features of this environment over geologic timescales.

Sample collection:

Samples were collected from 5 sites at OHK (Figure 2): Deep Source (1.2 m deep in the source pool at the borehole), Shallow Source (surface water and a thin biofilm along the edge of the source pool), Old Stream (water and thin biofilm along the semi-stagnant blocked outflow), Canal (along the flow from the source pool to the rotenburo), and Bubble Pool (downstream in a 15 cm deep pool coated in mineralized bubbles).

From, each site, both a "Mineral" and a "Water" sample were collected for 16S amplicon sequencing, targeting surface-associated and pelagic microbial communities, respectively. "Mineral" samples consisted of scrapings of thin biofilms, mineral precipitates, or whole mineralized bubbles from surfaces of travertines or cobbles in the bottom of water channels. Mineral samples were collected using sterile forceps and spatulas (~0.25 cm^3 of material). "Water" samples consisted of cells and sediment filtered from water using sterile syringes and 0.2 micron Sansyo (Sansyo Co., Tokyo, JP) filters (~50-200 ml of water filtered, until filter began to clog). Cells were lysed and DNA preserved in the field using Zymo Terralyzer BashingBead Matrix and Xpedition Lysis Buffer (Zymo Research, Irvine, CA). Cells were disrupted immediately by attaching tubes to the blade of a cordless reciprocating saw (Black & Decker, Towson, MD) and operating

for 1 minute. Samples for geochemical analysis consisted of water collected via sterile syringe and filtered immediately through a 0.2 micron Sansyo filter.

Geochemical analysis:

Dissolved oxygen (DO), pH, and temperature measurements were performed *in situ* using an Extech DO700 8-in-1 Portable Dissolved Oxygen Meter (FLIR Commercial Systems, Inc., Nashua, NH). Iron concentrations were measured using the ferrozine assay (Stookey 1970) following acidification with 40 mM sulfamic acid to inhibit iron oxidation by O_2 or oxidized nitrogen species (Klueglein and Kappler 2013). Ammonia/ammonium concentrations were measured using a TetraTest NH_3/NH_4^+ Kit (TetraPond, Blacksburg, VA) following manufacturers instructions but with colorimetry of samples and NH_4Cl standards quantified with a Thermo Scientific Nanodrop 2000c spectrophotometer (Thermo Fisher Scientific, Waltham, MA) at 700 nm to improve sensitivity and accuracy. Anion concentrations were measured via ion chromatography on a Shimadzu Ion Chromatograph (Shimadzu Corp., Kyoto, JP) equipped with a Shodex SI-90 4E anion column (Showa Denko, Tokyo, JP).

Total Organic Carbon (TOC) contents were assessed for filtered water and mineral precipitates from the source pool, as well as mineral precipitates near the canal. For dissolved organic carbon measurements, 3 liters of spring water was filtered using 0.45 micron Sansyo glass fiber filters. For mineral precipitates, approximately 300 g samples were collected. Carbonate carbon was removed via dissolution with HCl, and residues were folded into tin capsules and analyzed for carbon content via elemental analyzer (Thermoscientific Flash 2000) with a detection limit of 0.005% C by weight.

Samples of sediment from the source pool were characterized via SEM-EDS (SU5500; Hitachi, Tokyo, JP) and μM X-ray diffraction by TEM (JEM-3010; JEOL, Tokyo, JP).

Sequencing and analysis:

Following return to the lab, DNA was extracted and purified with a Zymo Soil/Fecal DNA extraction kit. The V4-V5 region of the 16S rRNA gene was amplified from each extract as well as negative controls using archaeal and bacterial primers 515F (GTGCCAGCMGCCGCGGTAA) and 926R (CCGYCAATTYMTTTRAGTTT) (Caporaso et al., 2012). DNA was quantified with a Qubit 3.0 fluorimeter (Life Technologies, Carlsbad, CA) according to manufacturer's instructions following DNA extraction and PCR steps. All samples yielded PCR amplicons when viewed on a gel after initial pre-barcoding PCR (30 cycles). Duplicate PCR reactions were pooled and reconditioned for five cycles with barcoded primers. Samples for sequencing were submitted to Laragen (Culver City, CA) for analysis on an Illumnia MiSeq platform. Sequence data were processed using QIIME version 1.8.0 (Caporaso et al., 2010). Raw sequence pairs were joined and quality-trimmed using the default parameters in QIIME. Sequences were clustered into de novo operational taxonomic units (OTUs) with 99% similarity using UCLUST open reference clustering protocol (Edgar, 2010). Then, the most abundant sequence was chosen as representative for each *de novo* OTU (Wang et al., 2007). Taxonomic identification for each representative sequence was assigned using the Silva-115 database (Quast et al., 2013) clustered at separately at 99% and at 97% similarity. Singletons and contaminants (OTUs appearing in the negative control datasets)

were removed. 16S sequences were aligned using MAFFT (Katoh et al. 2002) and a phylogeny constructed using FastTree (Price et al. 2010). Alpha diversity was estimated using the Shannon Index (Shannon 1948) and Inverse Simpson metric (1/D) (Simpson 1949; Hill 1973). All statistics were calculated using scripts in QIIME and are reported at the 99% and 97% OTU similarity levels. Multidimensional scaling (MDS) analyses and plots to evaluate the similarity between different samples and OHK environments were produced in R using the vegan and ggplot2 packages (R Core Team 2014, Oksanen et al. 2016, Wickham 2009).

Results and Discussion:

Geochemistry:

Geochemistry measurements of OHK source water are summarized in Table 1, while geochemical gradients along the stream outflow are summarized in Figure 3. Water emerging from the source was 44.3°C, very low in dissolved oxygen (<15 μM), had a pH 6.8, and contained substantial concentrations of dissolved iron (114 μM Fe^{2+}), and 22 μM NH_3/NH_4^+. After emerging from the borehole, the spring water rapidly exchanges gases with the air due to turbulent mixing associated with water flow and CO_2 ebullition, and DO rose to 30 μM in the shallow source pool. Dissolved organic carbon in the source pool was below the limit of detection (0.005% C by weight). Organic carbon content of mineral precipitates at the source pool was 0.01% by weight, rising to 0.02% near the canal. SEM-EDS analysis of source pool precipitates detected Fe and O as the major elements, and selected area X-ray diffraction by TEM revealed amorphous Fe-hydroxides as the solid phase with no detection of hematite or other crystalline phases (Figure 4). As water flows

downstream from the source pool, it cools slightly, degases CO_2, and continues to absorb atmospheric O_2. By the time water reaches the bubble pool, the spring water is 40°C, pH 7.5, and contains 7.7 μM NH_3/NH_4^+, 109 μM O_2 and no detectable dissolved iron. Concentrations of major anions were largely stable along the spring outflow, with 1350 mg/l Cl^-, 620 mg/l SO_4^{2-}, and no detectable NO_2^-, NO_3^-, or HPO_4^-.

Like many modern BIF analog hot spring sites, under the environmental conditions at OHK, abiotic iron oxidation is expected to proceed spontaneously. Following rate equations for abiotic iron oxidation from Singer and Stumm (1970), the rate of abiotic iron oxidation proceeds proportionately to concentrations of dissolved Fe^{2+}, O_2, and the activity of OH^-, of the form $-d[Fe^{2+}]/dt=k[Fe^{2+}]P_{O2}[OH^-]^2$, where k is a rate constant equal to about $8x10^{13}$ $liter^2$ $mole^{-2}$ atm^{-1} min^{-1}at 25°C, and increasing approximately 10-fold for every 15°C of temperature increase (Stumm and Lee 1961). In the deep source pool, where $[O_2]$ was below the detection limit of 0.5 mg/L (~15 μM), abiotic iron oxidation rates are therefore expected to be less than ~4.35 μM/min. This expected rate would be expected to increase between ~8.7 μM/min in the shallow source pool to ~12.7 μM/min in the canal, the last sampling location at which dissolved iron was detectable. These values are significant, and as a result abiotic iron oxidation likely contributes substantially to the production of iron oxides at OHK. Nonetheless, the abundance of iron oxidizing bacteria and morphology of iron oxide precipitates (below) demonstrates that there is a viable and active niche for biological iron oxide production. This is further supported by estimates of flow rates through OHK correlated against changes in iron oxide abundance from the edge of the Shallow Source Pool to the Canal, where flow rates of ~0.33 m/s through canals with

cross sections of ~10 cm by 5 cm suggest flow rates of ~1.67 L/s. Over distances of 2 m from the Shallow Source to the Canal, [Fe^{2+}] declines from ~114 μM to ~83 μM, or a change of 31 μM in approximately 6 seconds; this is equivalent to about 100-fold faster than expected for purely abiotic rates. Even assuming substantial backflow and mixing, this leaves a substantial role for aerobic iron oxidizing bacteria in explaining the decline in iron concentrations along the hot spring outflow. These results are also consistent with estimates from Kusama and Murakami (2001) that suggest aerobic iron oxidizing bacteria can increase iron oxidation rates by up to 4 orders of magnitude above those expected from purely abiotic reactions.

Recovered microbial diversity:

In total, we recovered 141,125 sequences from the 10 samples at OHK (Table 2). Reads per sample ranged from 2,176 for the Canal Mineral sample to 27,454 reads for the Old Stream Mineral sample (median 15,247, mean 14,112, and standard deviation 8,654). With the exception of the Old Stream Mineral sample, water samples consistently recovered more sequence reads than mineral samples (mean of 5,926 versus 18,983). Assessment of sampling depth was estimated using Good's Coverage (Good 1953). On average, 90% of the microbial community was recovered from OHK samples at the 99% OTU level (ranging from 75% coverage in the Canal Mineral sample to 96% in the Old Stream Mineral sample) and 94% at the 97% OTU level (83% for the Canal Mineral sample to 98% for the Old Stream sample).

Most of the taxonomic and abundance variation was related to location along the outflow and therefore the local environmental and redox conditions and consequent metabolic opportunities (Figure 3, Figure 5). The community composition of the water samples all appeared relatively similar to each other, with low dissimilarity between water samples and mineral samples from the source pool. Downstream, mineral samples appear dissimilar both from water samples and from each other (Figure 5).

Relative abundances of microbial taxa as revealed by 16S surveys can be useful for predicting metabolisms driving geochemical cycles and producing the mineral deposits observed at OHK (Table 3 and Figure 3). In particular, the contributions of various iron oxidizers and phototrophs to primary productivity along the spring path (Figure 3) can be estimated due to these metabolisms being fairly well conserved within bacterial taxa (e.g. Emerson et al. 2010, Chan et al. 2016). Analysis of the most abundant taxa at OHK revealed significant roles for organisms with diverse iron metabolisms, including aerobic and phototrophic iron oxidation, as well as trace iron reducers. While the relative contribution of abiotic iron oxidation at OHK is not constrained, sequence data suggest that aerobic iron oxidizing bacteria are the dominant biological drivers of iron oxidation in the hot spring. Also present were diverse phototrophs associated with both oxygenic and anoxygenic phototrophic clades; these organisms were observed at only trace abundance in most samples, but anoxygenic phototrophs were enriched in biofilms from the Old Stream, the rim of the Source Pool, while Cyanobacteria were abundant in the Bubble Pool. A small but diverse assortment of microbes associated with nitrogen cycling was present at

OHK, despite low concentrations of nitrogen compounds in the spring water (Supplementary Information)

Aerobic iron-oxidizing bacteria:

Among the most abundant taxa at OHK are members of the betaproteobacterial family Gallionellaceae, most likely members or close relatives of the aerobic iron-oxidizing genera *Gallionella* or *Sideroxydans*. *Gallionella* and *Sideroxydans* are neutrophilic iron oxidizers that use molecular oxygen to oxidize dissolved Fe(II) to Fe(III) oxides while conserving energy for growth and autotrophic carbon fixation (Kucera and Wolfe 1957, Emerson and Moyer 1997, Emerson et al. 2013); they are commonly found in terrestrial iron-rich systems (Emerson et al. 2010). Aerobic iron-oxidizing bacteria have characteristically low growth yields (Neubauer et al. 2002) due to the modest potentials of Fe(II)/Fe(III) redox couples and resulting requirement for reverse electron transfer to achieve the sufficiently low potential electrons needed for carbon fixation (Bird et al. 2011).

Gallionellaceae are abundant in both the mineral and water fractions of the Deep Source (37 and 18%, respectively), but otherwise appear to be dominantly associated with the water fraction of other samples (28% average in water samples, 8.5% average in mineral samples)(Table 3). This suggests that these organisms are predominantly planktonic or associated with suspended sediment particles rather than forming biofilms on stationary mineral surfaces. Based on the sequence data, members of the Gallionellaceae appear to be the first iron oxidizers and primary producers to act on the upwelling spring water as it mixes with atmospheric O_2, driving the bulk of early biological iron oxidation at

OHK and producing much of the iron oxide sediment that is transported along the spring outflow. Gallionellaceae were fairly diverse, including 169 OTUs at the 97% identity cutoff; however, the two most abundant OTUs were both ~97% similar to *Sideroxydans lithotrophicus* ES-1, and represented more than 92% of the total Gallionellaceae sequences at OHK. The abundance of these two OTUs drives the overall trend in iron oxidizer abundance (Figure 3).

Also present, albeit at lower abundance (up to ~1.5% relative abundance)(Table 3), are members of the zetaproteobacterial family Mariprofundaceae, another group of neutrophilic iron oxidizers. Iron-oxidizing Zetaproteobacteria are more commonly found in marine settings, particularly in deep ocean basins associated with hydrothermal iron sources (Emerson et al. 2010). Despite a similar physiology, Mariprofundaceae are not closely related to Gallionellaceae or other aerobic iron oxidizers, instead forming a distinct class within the Proteobacteria (Emerson et al. 2007). Zetaproteobacteria have previously been identified in relatively saline terrestrial iron- and CO_2-rich systems (e.g. Emerson et al. 2016), sometimes co-occurring with *Gallionella* (Crossey et al. 2016); the discovery of the co-occurrence of these organisms at OHK provides further support to the overlapping ecological niches of these classically "marine" and "terrestrial" iron oxidizing bacteria.

Members of the Gallionellaceae are typically associated with cold iron-oxidizing environments, and not hot springs (Delong et al. 2014), while members of the Mariprofundaceae have been observed to have an upper growth temperature of 30°C (Emerson et al. 2010). OHK, with source water temperatures ~44°C may therefore support unique thermotolerant strains of these bacteria.

Members of the family Comamonadaceae were also fairly abundant (~1-12%) in OHK samples (Table 3). This family of Betaproteobacteria includes members such as *Acidovorax ebreus,* a nitrate-reducing anaerobic iron oxidizer (Byrne-Bailey et al. 2010), as well as iron reducers such as *Rhodoferax ferrireducens* (Finneran et al. 2003) and the iron-oxidizing bacterium *Leptothrix* (van Veen et al. 1978). However, the taxonomic affinity of the Comamonadaceae at OHK is insufficiently resolved to confidently assess the contribution of this group to iron cycling in this environment.

Electron microscopy of mineral precipitates from the source pool and canal revealed alternating laminations of aragonite-rich and iron-oxide-rich material; imaging of iron oxide bands following dissolution of carbonates with HCl revealed that iron oxides were made up of a mixture of amorphous and sheath-like tubular structures (Figure 4). While iron oxide sheaths are typically associated with the betaproteobacterial iron-oxidizing genus *Leptothrix* (Emerson et al. 2010), they can also be produced by diverse iron oxidizers including some strains of Zetaproteobacteria (Fleming et al. 2013). Though we tentatively regard these mineralized filaments as biological in origin, it is unclear what organisms are responsible for the production of iron oxide sheaths observed at OHK. Sub-micron, amorphous particulate iron oxides are characteristic of iron oxidation by *Sideroxydans* (Emerson and Moyer 1997), and so the prevalence of this iron-oxide morphology is consistent with this genus of the Gallionellaceae being major contributors to iron oxidation at OHK. The abundance of amorphous iron oxide particles also supports the assignment of Gallionellaceae OTUs at OHK to *Sideroxydans* rather than stalk-forming *Gallionella* (Emerson et al. 2010).

Cyanobacteria:

Cyanobacteria were abundant in the Bubble Pool Water sample, where they made up ~37% of all sequence reads, but were of much lower abundance in samples collected upstream (Table 3 and Figure 3). Though Cyanobacteria are sometimes underrepresented in iTag datasets as a result of poor DNA yield or amplification biases (e.g. Parada et al. 2015, Trembath-Reichert et al. 2016), the paucity of Cyanobacteria in upstream OHK samples was confirmed by fluorescent microscopy, in which cells displaying cyanobacterial autofluorescence were observed abundantly in samples from the downstream Bubble Pool samples but not in the Source Pool (Supplementary Figure 2).

It has been demonstrated that in iron-rich systems where Cyanobacteria are abundant and productive, only ~1% of O_2 released oxidizes ferrous iron, with the remainder escaping to the atmosphere (Rantamäki et al. 2016). Thus, given the inefficiency of cyanobacterial oxygen fluxes for oxidizing dissolved iron, and the scarcity of Cyanobacteria upstream at OHK where iron oxidation is taking place, Cyanobacteria do not appear to be major contributors to iron oxidation at OHK.

Cyanobacteria present are predominantly members of Subsection III, Family I. This group includes *Leptolyngbya*, a genus of filamentous non–heterocystous Cyanobacteria that has appeared in clone libraries from OHK (Takashima et al. 2011) and is common in other hot springs of similar temperatures (e.g. Roeselers et al. 2007, Bosak et al. 2012).

Members of deeply branching nonphototrophic Cyanobacteria clades are a minor but notable component of OHK samples (up to 0.9% abundance). While the Cyanobacteria phylum has traditionally been considered to exclusively contain oxygenic phototrophs,

several deep-branching nonphototrophic clades have recently been described within the Cyanobacteria phylum, including Melainabacteria, a sister group to oxygenic Cyanobacteria (i.e. Oxyphotobacteria), as well as deeper-branching clades (Ley et al. 2005, Di Rienzi et al. 2013, Johnson et al. 2013b, Soo et al. 2014, Soo et al. 2015). These deep-branching Cyanobacteria—particularly the clades SHA-109 and ML635J-21, which branch basal to all other Cyanobacteria—are thought to be ancestrally nonphototrophic, and can help to better constrain the evolutionary history of Cyanobacteria and therefore oxygenic photosynthesis (e.g. Shih et al. 2016, Fischer et al. 2016, Soo et al. 2017). These clades are found at higher abundance at OHK than most other environments, and OHK could provide a valuable resource for investigating members of this understudied group via metagenomic sequencing, incubations, or isolation.

Anoxygenic phototrophs and relatives:

Members of several taxa made up of or containing anoxygenic phototrophs were present at low abundance in OHK samples (Table 3). These include the Rhodospirillalles, Rhodobacteraceae, Rhodocyclaceae, Chloroflexaceae, Chlorobiales, and Chromateaceae. Some of these taxa (e.g. Chloroflexaceae, Chlorobiales) are made up almost exclusively of phototrophs, while others (e.g. Rhodobacteraceae) contain members with a wide diversity of metabolisms, only some of which are phototrophic (Overmann and Garcia-Pichel 2013, Fischer et al. 2016). Shotgun metagenomic or culture-based analysis will be necessary to confirm whether the members of these taxa present at OHK are phototrophic. Though these taxa individually represent no more than a few percent of the sequence reads at any given site (overall average ~0.88% of reads per taxon), this population is quite diverse and in sum

represents a sizable fraction of the total microbial community (3-20%)(Figure 3). Putative anoxygenic phototrophs are most abundant in the Shallow Source and Old Stream mineral samples (13.8% and 20.4% of total abundance, respectively), dropping to ~3% in the Deep Source sample. Even in the downstream Bubble Pool samples, anoxygenic phototrophs make up ~5% of the total abundance of sequences. Sequences associated with anoxygenic phototrophs were more abundant in mineral samples than in water samples (~9% vs. ~5%), suggesting that these organisms grow preferentially attached to solid surfaces rather than planktonically.

All samples contained relatively abundant sequence reads belonging to the Chlorobi phylum (Table 3). The Chlorobi are classically known as the Green Sulfur Bacteria due to the anaerobic sulfur-oxidizing anoxygenic phototrophic lifestyle of its earliest described members (Davenport et al. 2010, Bryant and Liu 2013). This includes iron-oxidizing anoxygenic phototrophs such as *Chlorobium ferrooxidans* (Heising et al. 1999), which employ a metabolism thought to be relevant to Archean BIF deposition (e.g. Kappler et al. 2005). Due to increased environmental sequencing and new isolation efforts, however, the Chlorobi phylum is now known to also contain aerobic photoheterotrophs (Liu et al. 2012b, Stamps et al. 2014) and nonphototrophs (Podosokorskaya et al. 2012). The majority of Chlorobi sequences found in OHK appear to fall within the Chlorobi order Ignavibacteria, a basal clade of Chlorobi whose known members include versatile heterotrophic metabolisms but no known phototrophy pathways (Iino et al. 2010, Liu et al. 2012a). It therefore appears that photoferrotrophy by Chlorobi is not driving iron oxidation at OHK, though metagenomic sequencing and assembly of OHK Chlorobi genomes will be

necessary to confirm that phototrophy is not present in these organisms. Ignavibacteria appear to be a common component of hot spring microbial communities: these organisms were first isolated from a Japanese hot spring (Iino et al. 2010), and are found at high abundance in Chocolate Pots hot springs in Yellowstone National Park (Fortney et al. 2016).

The Ignavibacteria found at OHK had only low similarity to described strains, with more than 50% of Ignavibacteria reads (primarily from the Deep Source and Canal Water samples) from an OTU ~91% similar to *Melioribacter roseus* P3M, a moderately thermophilic facultative anaerobe (Kadnikov et al. 2013). Approximately 20% of Ignavibacteria reads (primarily from the Deep Source Water and Old Stream Mineral samples) were 93% similar to *Ignavibacteria album* JCM 16511.

Members of the bacterial phylum Chloroflexi were remarkably abundant in OHK samples (Table 3). The Chloroflexi were classically been described as the Green Nonsulfur Bacteria due to the anoxygenic phototrophic metabolism of their earliest described members (Overmann 2008), but it is now recognized that the phylum is much more genetically and metabolically diverse (Yamada and Sekiguchi 2009). Metabolic characters in the Chloroflexi largely follow class-level taxonomic patterns but with a number of notable exceptions, such as the nonphototrophic predatory *Herpetosiphon* within the predominantly phototrophic Chloroflexia class (Kiss et al. 2011, Ward et al. 2015b). The most abundant Chloroflexi at OHK belong to the class Anaerolineae, which were abundant in all samples (up to ~11%). The Anaerolineae have generally been isolated as obligately anaerobic heterotrophs (e.g. Sekiguchi et al. 2003, Yamada et al. 2006), but genome

sequencing has revealed the capacity for aerobic respiration in diverse members of this clade (e.g. Hemp et al. 2015a, Hemp et al. 2015b, Pace et al. 2015, Ward et al. 2015a). Furthermore, a genome for an organism closely related to the Anaerolineae with genes for photosynthesis has been assembled from a Yellowstone National Park metagenome (Klatt et al. 2011). It is therefore unclear what metabolisms may be present in Anaerolineae at OHK, and isolation or metagenomic sequencing of these organisms will be necessary to determine what role they may be playing in this environment. The Anaerolineae at OHK were very diverse, including 480 OTUs at the 97% cutoff. This included a distinct population at the Deep Source (both Water and Mineral Samples), the Shallow Source Mineral sample, and more downstream samples. The three most abundant Anaerolineae OTUs were most closely related to *Thermomarilinea lacunifontana* (84-88% similarity); *T. lacunifontana* is an anaerobic heterotroph isolated from a shallow hydrothermal system in Japan (Nonoura et al. 2013). The most abundant Anaerolineae OTU in the Shallow Source Water sample (making up ~7% of all Anaerolineae at OHK) was 89% identical to *Ornatilinea apprima*. The most abundant OTU in the Old Stream Mineral sample was 91% identical to *Longilinea arvoryzae*. Both *O. apprima* and *L. arvoryzae* are described as obligately anaerobic fermenters capable of degrading sugars and proteins (Yamada et al. 2007, Podosokorskaya et al. 2013).

Conclusions:

OHK is a unique ecosystem supporting novel microbial communities as well as serving as an intriguing process analog for Precambrian banded iron formation deposits. Future activity measurements of community members, for example by metagenomics and

stable isotope probing will be necessary to further define microbial activities in this system. Based on microscopy and 16S amplicon data, the microbial communities at OHK appear to be supported primarily by aerobic iron oxidation occurring in and near the source pool. In the old stream, mineral attached anoxygenic phototrophs become more significant, while Cyanobacteria become abundant only in the most downstream samples. This predominance of lithoautotrophs over phototrophs is rare at the Earth's surface today, and provides a contrast to other modern BIF analog sites. For instance, in Lake Matano iron oxidation is thought to be driven largely by photoferrotrophs (Crowe et al. 2008). At Chocolate Pots hot spring in Yellowstone National Park—perhaps the most geochemically-similar system to OHK that has been extensively studied—iron oxidation is thought to be primarily driven abiotically by O_2 produced *in situ* by cyanobacterial mats (Trouwborst et al. 2007). Furthermore, relative to Chocolate Pots, OHK supports very little in the way of well-developed microbial mats, with only thin, patchy biofilms.

The absence of substantial microbial biomass accumulation near the source pool at OHK can be considered the result of two separate phenomena: 1) the paucity of photosynthetic Cyanobacteria, and 2) the poor growth yields of the iron-oxidizing bacteria that do occur. Neither of these issues is fully resolved, but hypotheses for their causes can be made based on the geochemistry and mineralogy of OHK and related systems, as well as aspects of the physiologies driving iron oxidation.

It has been proposed that high iron concentrations are toxic to Cyanobacteria, and that this may have played a role in delaying the oxygenation of the Archean atmosphere (Swanner et al. 2015). In principle, ferrous iron toxicity may help explain the absence of

Cyanobacteria in OHK until the most downstream samples, where most iron has already been oxidized and precipitated. The absence of Cyanobacteria at OHK is challenging to explain, however, as other iron-rich systems (e.g. Chocolate Pots Hot Spring, Trouwborst et al. 2007) support productive cyanobacterial populations, and in other systems oxygenic photosynthesis and aerobic iron oxidation have been shown to co-occur (Hegler et al. 2012, Mori et al. 2015). At Fuschna Spring in the Swiss Alps, *Gallionella*-dominated communities occur in the iron-rich, low-oxygen, high-flow conditions within the flow channel, but Cyanobacteria- and iron reducer-rich microbial mats accumulate along the edges where flow is less pronounced (Hegler et al. 2012). This suggests that flow regime may also play a role in determining the microbial community of iron-rich systems; OHK experiences high flow rates, and turbulent mixing in the source pool, and this may play a role in limiting the development of phototrophic microbial mats. Turbulence may inhibit the development of phototrophic microbial mats, while simultaneously being advantageous to aerobic iron oxidizing bacteria by helping them shed accumulated iron oxides, limiting encrustation by their metabolic byproducts.

A reasonable hypothesis for the poor development of biofilms by aerobic iron oxidizing bacteria at OHK could be related to the low growth yield of aerobic iron-oxidizing microbes relative to phototrophs. Based on electron balance for an average oxidation state of zero for organic carbon, the maximum possible efficiency of autotrophic iron oxidation is 1 mole of CO_2 fixed for every 4 moles of Fe(II) oxidized. However, measured yields of aerobic iron oxidizers are typically much lower, on the order of 1 mole of CO_2 fixed for every 40 moles of Fe(II) oxidized (Neubauer et al. 2002). Yields for

photoferrotrophs appear to be much more efficient, approximating the ideal stoichiometry of 4 Fe: 1 C (Ehrenreich and Widdel 1994). While electron transfer in neutrophilic iron oxidizers has not been extensively characterized, this difference in yield appears to fundamentally come down to the redox potential of iron oxidation reactions, which (while quite variable depending on environmental pH and mineralogy of iron oxides) are too electrochemically positive to directly reduce $NAD(P)^+$ and therefore be useful for carbon fixation (Bird et al. 2011). In order to grow, these organisms must consume proton motive force (PMF) to run electrons "uphill" to lower redox potentials in order to generate the NAD(P)H needed to reduce CO_2 (Bird et al. 2011). In aerobic iron oxidizers, this requires large fluxes of iron oxidation to maintain sufficient PMF to fix carbon, while phototrophic iron oxidizers can rely on cyclic electron flow through their reaction centers to build PMF sufficiently to allow stoichiometric iron oxidation and carbon fixation. This relatively poor growth yield of aerobic iron oxidizing bacteria at OHK results in organic carbon-lean mineral precipitates (<0.02% organic carbon by weight), in contrast to phototroph-dominated iron-rich systems like Chocolate Pots hot spring where organic carbon contents can be in excess of 1% organic carbon by weight (Parenteau and Cady 2010). Ultimately it is the overproduction of ferric iron relative to carbon fixation during aerobic iron oxidation that sets the budgets for subsequent carbon and iron cycling in the environment.

Significantly, 16S sequence reads associated with environmentally common iron-reducing microbes (e.g. Shewanellaceae, Geobacteraceae) occur at only very low abundances at OHK, with a maximum abundance of the Deltaproteobacteria family Geobacteraceae of 0.79% in the Deep Source Water sample (Table 3). This is in contrast to

other iron rich, neutral pH systems including hot and cold springs and groundwater seeps (e.g. Hegler et al. 2012, Blöthe and Roden 2009, Roden et al. 2012, Fortney et al. 2016). This may partially reflect the relative fluxes of iron oxidation versus organic carbon fixation at OHK; *i.e*. there is insufficient organic carbon being fixed in this environment to fuel substantial iron oxide respiration. Meanwhile, turbulent mixing ensures that oxygen-poor microenvironments do not develop. Since molecular oxygen is available in substantial excess of organic carbon, heterotrophy at OHK never depletes O_2 sufficiently to make iron oxides a favorable electron acceptor. In contrast, in systems with more substantially developed microbial mats or less efficient mixing, oxygen can become depleted deeper in mat fabrics or in diffusion-limited boundary layers, driving local anoxia and the shift toward iron respiration. The lack of substantial iron reduction at OHK is consistent with the predominance of ferric iron minerals in the OHK deposits (Takashima et al. 2011)(Figure 3).

The relative paucity of organic carbon, the dominantly ferric iron content of sedimentary laminations, and the primary role of aerobic iron oxidation together make OHK most similar to Proterozoic-type BIFs, deposited after the GOE. BIF composition varies through time, with BIFs of different ages likely forming via different processes. This variability is likely driven by changes in primary productivity and remineralization pathways caused by the evolution of oxygenic photosynthesis in Cyanobacteria and the subsequent oxygenation of the atmosphere at the GOE *ca*. 2.3 Ga. While substantial debate exists about the antiquity of Cyanobacteria, multiple lines of evidence suggest that oxygenic photosynthesis evolved only shortly before the GOE (Johnson et al. 2013a, Ward

et al. 2016, Fischer et al. 2016, Shih et al. 2016), and therefore molecular oxygen derived from photosynthesis was unlikely to play a role in Archean BIF formation. The hypothesis that the deposition of these BIFs occurred via phototrophic iron oxidation is consistent with the predominantly ferrous composition of Archean and early Paleoproterozoic iron formations (Fischer and Knoll 2009)(Supplementary Information), and is discordant with mechanisms relying on aerobic iron oxidation; photoferrotrophy results in stoichiometric amounts of iron oxide and organic carbon delivered to sediments, which promotes an environment conducive to substantial amounts of iron reduction during burial and diagenesis (Konhauser et al. 2005, Johnson et al. 2007, Li et al. 2013). After the GOE, molecular oxygen was sufficiently abundant in the atmosphere Earth surface environments that it could be used to drive aerobic iron oxidation. Additionally, it has been observed that the organic carbon content of BIF tends to be inversely correlated to the proportion of residual ferric iron, with the most iron oxide-dominated BIFs containing on the order of 0.01% or less organic carbon by weight (Klein 2005, Fischer et al. 2014). Proterozoic BIFs, such as the syn-glacial iron formations that co-occur with Snowball Earth episodes late in Neoproterozoic (Cryogenian) time (Kirschvink 1992, Hoffman et al. 1998), are dominantly comprised of ferric iron phases. This is consistent with expectations for their deposition via aerobic iron oxidation (i.e. excess deposition of iron oxides relative to organic carbon, limiting subsequent iron reduction), and most closely resembles the mineralogy of the materials currently being deposited at OHK. By contrasting OHK with other BIF process analog sites where iron oxidation predominantly occurs by different processes (e.g. phototrophy), it may be possible to open a window into the ecology, mineralogy,

productivity, and other aspects of BIF deposition across the GOE, with OHK representing an endmember in which the iron oxide component of BIF sediment was deposited primarily by aerobic iron oxidation.

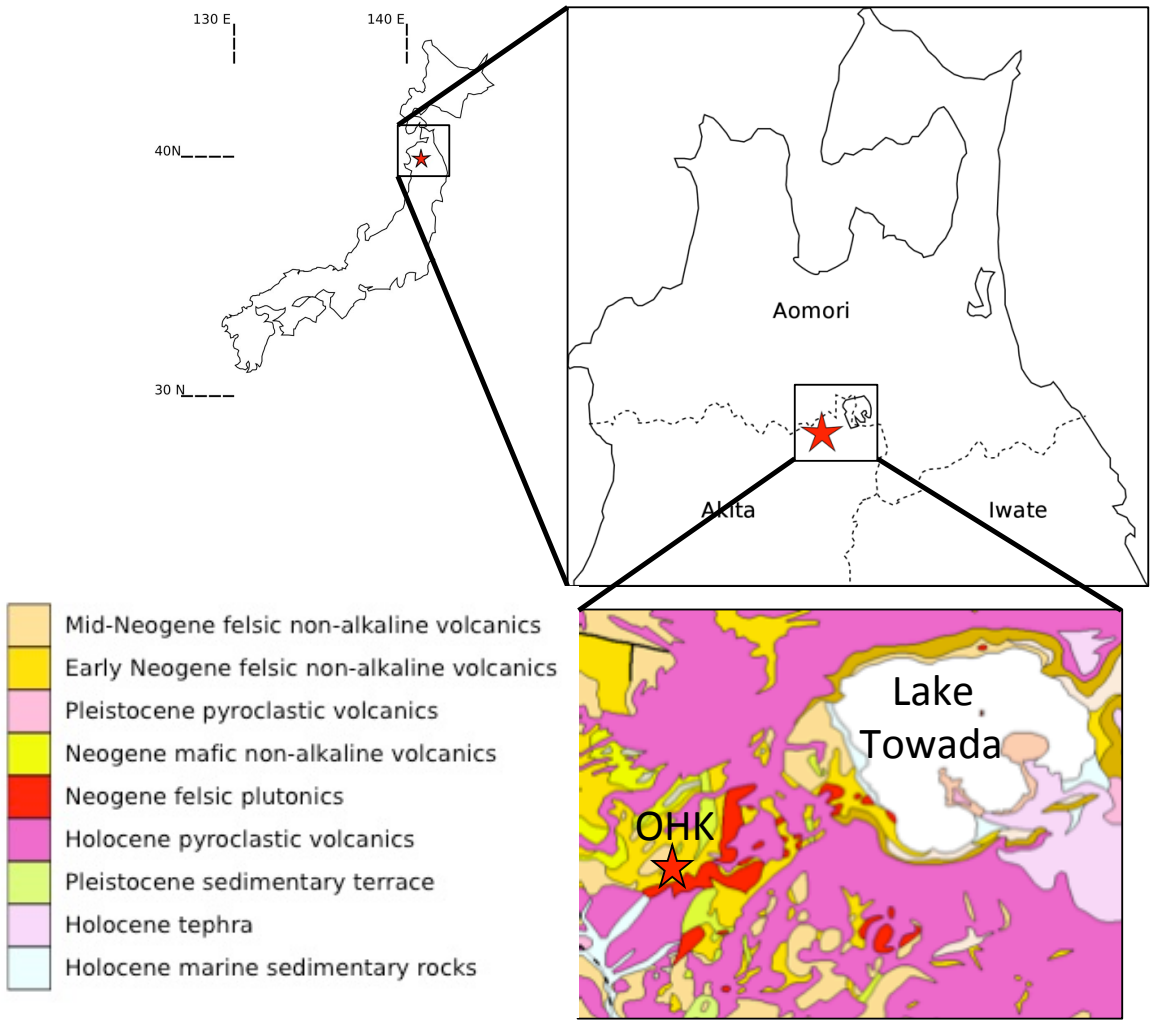

Figure 1: Location of Okuoku-hachikurou Onsen (OHK) in Akita Prefecture, Japan. Inset highlights the local geology of the Lake Towada region, modified from Geological Survey of Japan 2012. The bedrock geology at OHK consists predominantly of felsic volcanics.

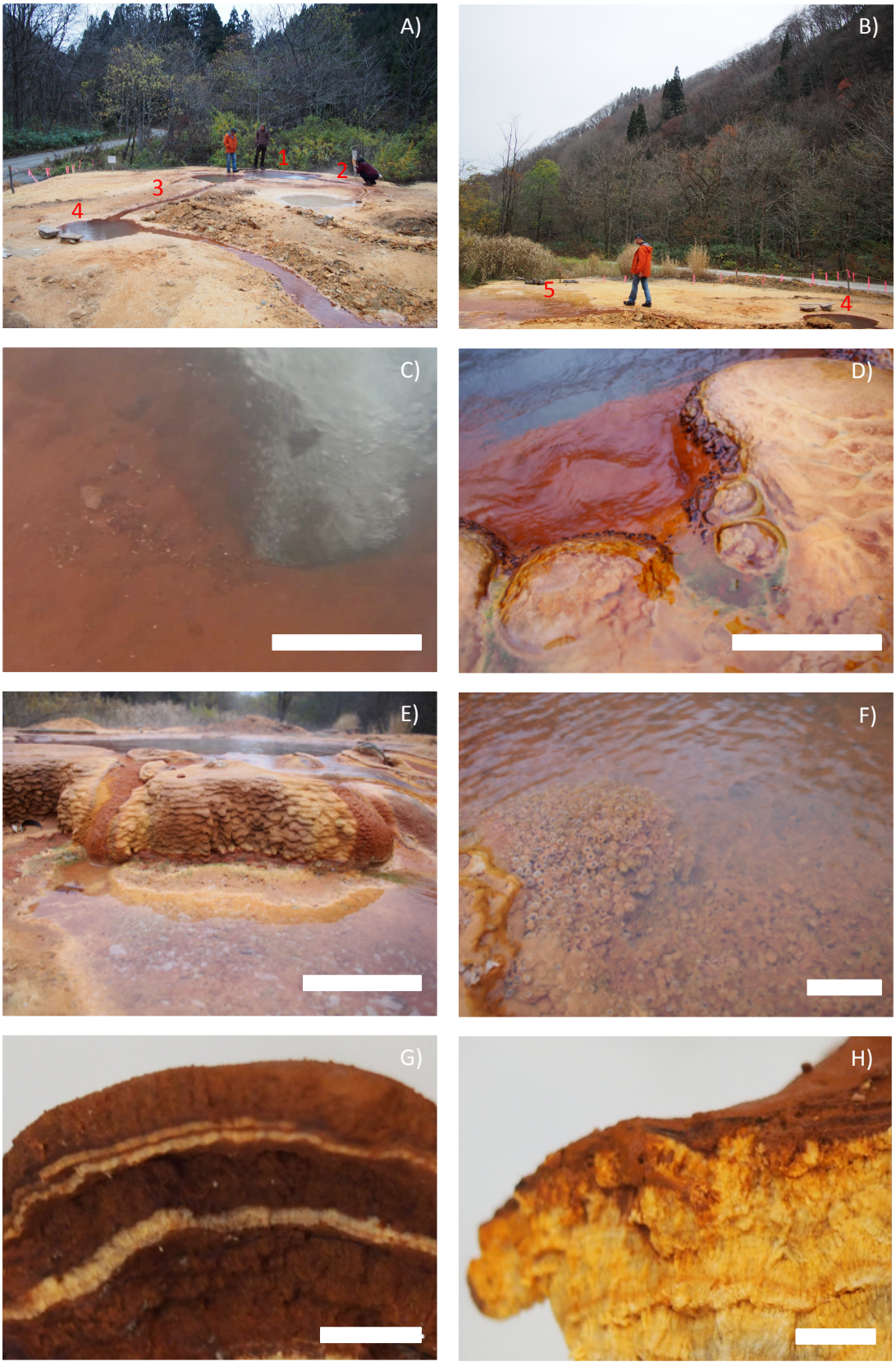
A)
1
2
3
4
B)
5
4
C)
D)
E)
F)
G)
H)

Figure 2: Context photographs of OHK. A) Photograph of OHK facing north toward source pool. Source pool (1), old stream (2), canal (3) and rotenburo (4) visible. People for scale (~1.8 m). B) Image of OHK facing southwest toward rotenburo and bubble pool. Water flowing from the rotenburo (4) develops into a sheeted flow which spreads across the hillside, filling the bubble pool (5) where degasing CO_2 bubbles become encrusted in aragonite. Person for scale (~1.8 m). C) Underwater photograph of source. Water and CO_2 bubbles emerge from the borehole at right. Scale bar is 10 cm. D) Lobate wall of travertine at the rim of the source pool, with green-pigmented biofilms (sampled as Shallow Source Mineral sample) visible. Scale bar is 10 cm. E) Close up of travertine on the west edge of the source pool. Scale bar is 50 cm. F) Close up photograph of the bubble pool, showing aragonite-mineralized CO_2 bubbles. Scale bar 5 cm. G,H) Close ups of ferrihydrite and aragonite laminations in travertine. Red layers are primarily composed of ferrihydrite, while white layers are predominantly aragonite. Scale bars shown are 5 mm.

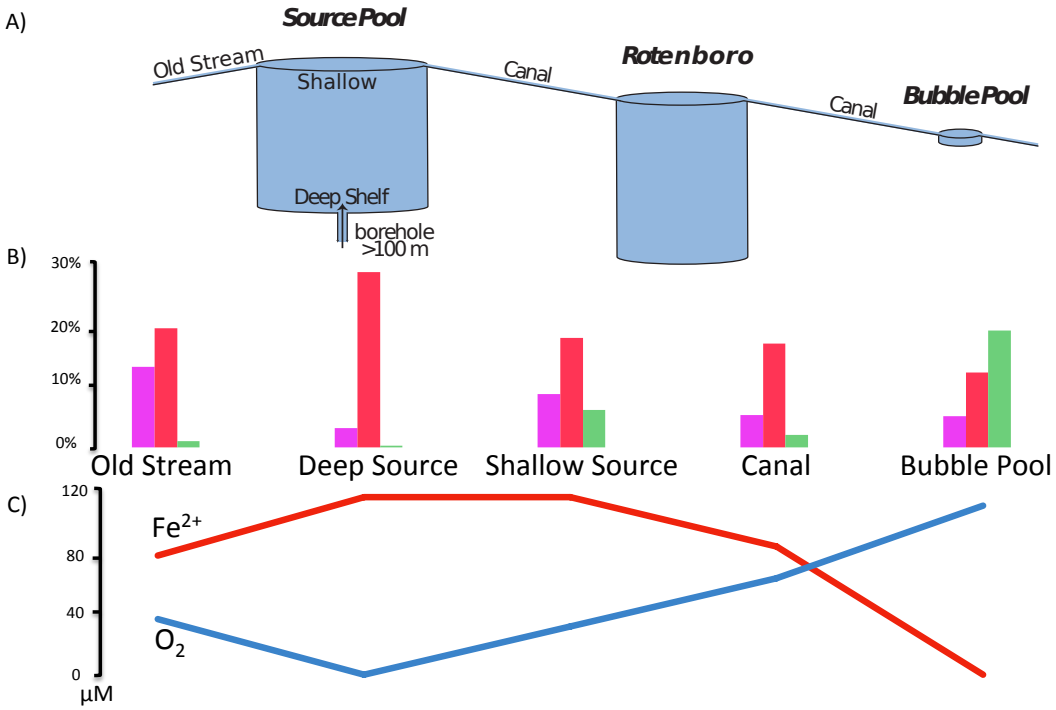

Figure 3: Summary of the geochemistry and iron-oxidizing community composition of OHK ordinated along the flow paths in the system. A) Schematic of OHK flow paths, keyed to the sample names. Mineral and Water samples were collected from Old Stream, Deep Source, Shallow Source, Canal, and Bubble Pool localities. B) Relative abundance of phototrophic and iron-oxidizing taxa along the flow path. Data here include taxa listed in Table 5 and discussed in the text with confidently assigned metabolisms, but not including taxa such as Anaerolineae whose metabolisms cannot be predicted with available taxonomic resolution. Relative abundance of taxa have been summed and then averaged per site between Mineral and Water samples. Aerobic iron oxidizers are shown in red, anoxygenic phototrophs in purple, and oxygenic Cyanobacteria in green. Aerobic iron oxidizers dominate near the source pool, while anoxygenic phototrophs are abundant in the Old Stream and Shallow Source Mineral samples, and oxygenic Cyanobacteria are highly

abundant only in the Bubble Pool Water sample. C) Concentrations of dissolved O_2 and Fe^{2+}. Source waters are depleted in O_2 but high in dissolved iron, while downstream Fe^{2+} concentrations drop and O_2 increases. The majority of iron oxidation appears to occur under microoxic conditions where aerobic iron oxidizers are most prevalent, while anoxygenic phototrophs are largely restricted to biofilms, and Cyanobacteria are only significant after the iron has already been removed from solution. Changes in temperature (44.3-40.7 °C) and concentrations of chloride (~37-39 mM) and sulfate (~6.3-6.65 mM) along the hot spring outflow were minor and not expected to contribute significantly to changes in microbial community or mineral precipitates, and so are not displayed here.

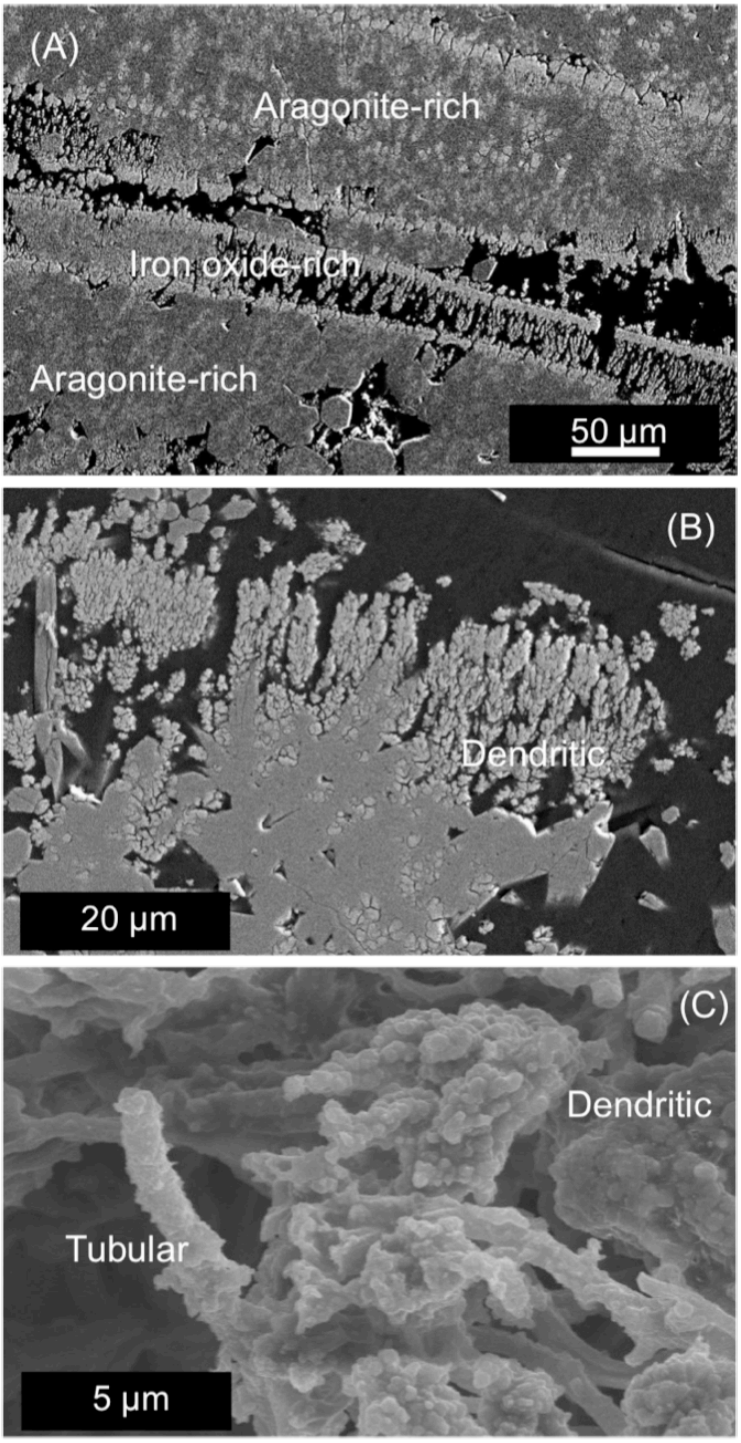

Figure 4: Electron microscopy imaging of precipitates from source pool. Back-scattered electron images collected by SEM of thin section samples of solids collected from

the travertine wall of the source pool (Figure 2D). This sample shows alternating laminations of aragonite-rich zones and iron oxide-rich zones. A) overview image illustrates alternation of carbonate- and iron oxide-rich layers. B) enlarged image of iron oxide-rich zone of A), showing aggregation of iron oxide nanoparticles into a dendritic texture. C) image of dendritic iron oxide aggregates following removal of carbonate phases via treatment with HCl, revealing sheath-like tubular and amorphous particulate iron oxide morphotypes.

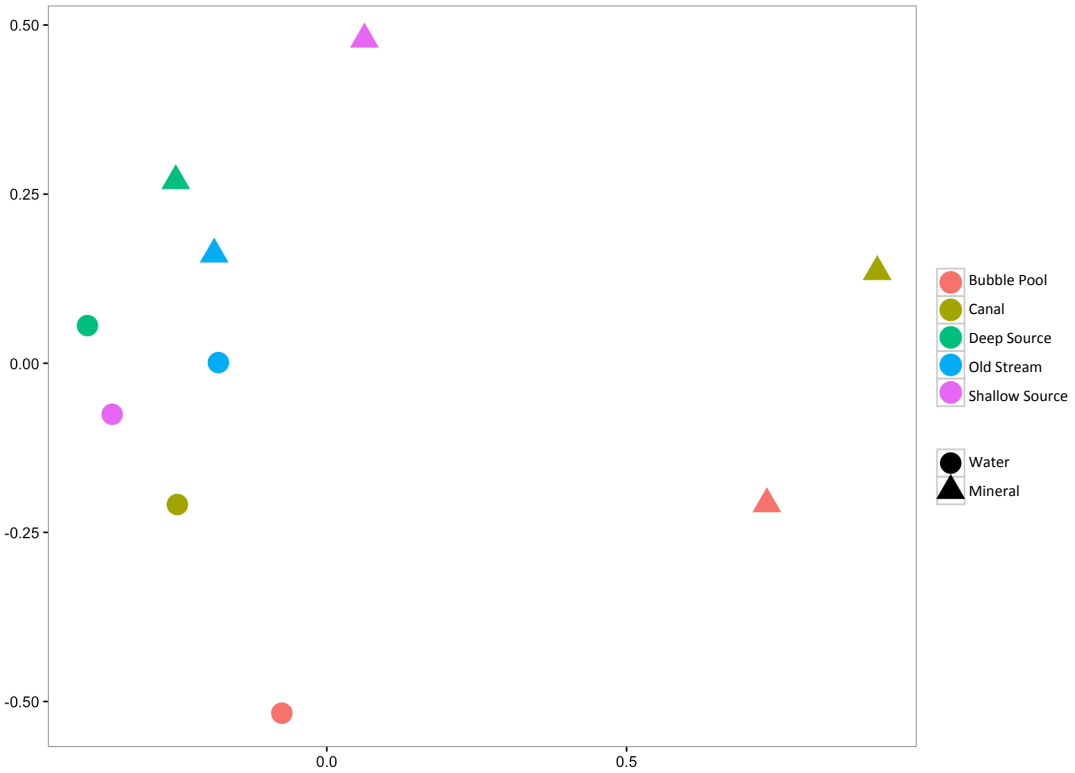

Figure 5: Multidimensional scaling analysis of OHK samples. Each point represents the recovered microbial community from a given sample, with sites identified by color and sample type by shape. Points close to each other in this two dimensional space share a similar community composition. Relative abundance data were transformed by the 4th root to down-weight the effect of abundant taxa in the samples. Water samples cluster together, and with Source pool mineral samples, while the Bubble Pool Water and the other Mineral samples stand out along different curves in this space. Stress value is 0.0465.

T	44.3°C
pH	6.8
DO	<15 μM
Fe^{2+}	114 μM
NH_3/NH_4^+	22 μM
Cl^-	38 mM
SO_4^{--}	6.5 mM
NO_3^-	b.d.
NO_2^-	b.d.
HPO_4^-	b.d.
TOC	b.d.

Table 1: Geochemical characteristics of OHK source water.

	Deep Source Mineral	Deep Source Water	Shallow Source Mineral	Shallow Source Water	Old Stream Mineral	Old Stream Water	Canal Mineral	Canal Water	Bubble Pool Mineral	Bubble Pool Water
Reads:	6456	20067	6512	25306	27454	19052	2176	17893	3608	12601
Observed OTUs (99%)	906	1928	1045	2450	1775	1842	740	2455	857	1595
Good Coverage (99%):	0.9035	0.9388	0.8948	0.941	0.9615	0.9423	0.7468	0.9076	0.8287	0.911
Shannon Index (99%):	5.9544	6.0339	7.6849	6.4785	6.8302	6.3403	8.113	6.8482	7.2747	5.896
Inverse Simpson (99%):	9.4959	12.9196	62.6337	11.5082	37.0168	11.4379	105.3153	12.7881	32.6025	8.6475
Observed OTUs (97%)	431	895	572	1059	747	869	490	1281	555	910
Goods Coverage (97%)	0.9588	0.9737	0.9459	0.9768	0.9834	0.9738	0.8359	0.9529	0.8911	0.951
Shannon Index (97%)	4.7603	4.6789	6.4739	5.0554	5.5785	5.0959	7.0603	5.4767	6.1736	4.5711
Inverse Simpson (97%):	6.5623	8.4309	33.1331	7.5288	22.6658	7.7054	55.6231	8.1763	18.5504	5.567

Table 2: Diversity metrics of OHK sequencing. Diversity metrics calculated for both 99% and 97% sequence identity cutoffs for assigning OTUs.

Taxon	Deep Source Mineral	Deep Source Water	Shallow Source Mineral	Shallow Source Water	Old Stream Mineral	Old Stream Water	Canal Mineral	Canal Water	Bubble Pool Mineral	Bubble Pool Water	Average
Bacteria;_Proteobacteria;_Betaproteobacteria;_Nitrosomonadales;_Gallionellaceae	36.94%	18.23%	1.09%	34.05%	3.27%	33.57%	0.46%	31.77%	0.44%	23.58%	18.34%
Bacteria;_Proteobacteria;_Zetaproteobacteria;_Mariprofundales;_Mariprofundaceae	0.65%	1.32%	0.05%	0.52%	1.51%	0.52%	1.01%	0.58%	0.17%	0.17%	0.65%
Bacteria;_Cyanobacteria;_Cyanobacteria;_SubsectionIII;_FamilyI	0.15%	0.24%	2.50%	4.46%	0.21%	1.41%	0.46%	2.30%	0.33%	37.45%	4.95%
Bacteria;_Cyanobacteria;_Cyanobacteria;_SubsectionV;_FamilyI	0.08%	0.11%	0.09%	5.16%	0.01%	0.31%	0.00%	1.29%	0.06%	0.20%	0.73%
Bacteria;_Proteobacteria;_Alphaproteobacteria;_Rhodospirillales;Other	0.09%	0.05%	6.68%	0.04%	2.57%	0.17%	0.09%	0.13%	0.19%	0.03%	1.00%
Bacteria;_Proteobacteria;_Betaproteobacteria;_Rhodocyclales;_Rhodocyclaceae	0.94%	0.55%	0.15%	0.42%	2.61%	3.31%	0.00%	0.99%	0.53%	0.38%	0.99%
Bacteria;_Proteobacteria;_Alphaproteobacteria;_Rhodobacterales;_Rhodobacteraceae	0.11%	0.34%	1.80%	0.47%	2.85%	0.26%	0.74%	0.87%	0.25%	0.14%	0.78%
Bacteria;_Proteobacteria;_Alphaproteobacteria;_Rhodospirillales;_Rhodospirillaceae	0.03%	0.01%	3.13%	0.04%	0.07%	0.06%	0.09%	0.30%	0.19%	0.29%	0.42%
Bacteria;_Chloroflexi;_Chloroflexia;_Chloroflexales;_Chloroflexaceae	0.00%	0.00%	0.05%	0.02%	0.00%	0.00%	1.19%	0.27%	0.83%	0.12%	0.25%
Bacteria;_Chlorobi;_Chlorobia;_Chlorobiales;_OPB56	0.09%	0.21%	0.06%	0.03%	0.17%	0.30%	0.14%	0.17%	0.03%	0.02%	0.12%
Bacteria;_Proteobacteria;_Gammaproteobacteria;_Chromatiales;_Chromatiaceae	0.42%	0.00%	0.00%	0.04%	0.00%	0.18%	0.00%	0.01%	0.03%	0.21%	0.09%
Bacteria;_Proteobacteria;_Gammaproteobacteria;_Xanthomonadales;_Xanthomonadaceae	0.22%	0.61%	3.06%	0.41%	10.01%	0.30%	9.33%	1.70%	24.89%	1.39%	5.19%
Bacteria;_Chloroflexi;_Anaerolineae;_Anaerolineales;_Anaerolineaceae	7.13%	10.75%	10.10%	3.52%	2.32%	0.91%	1.47%	3.67%	2.22%	0.60%	4.27%
Bacteria;_Proteobacteria;_Betaproteobacteria;_Burkholderiales;_Comamonadaceae	1.50%	1.88%	2.03%	2.35%	12.12%	1.51%	1.42%	4.15%	2.52%	4.38%	3.39%
Bacteria;_Nitrospirae;_Nitrospira;_Nitrospirales;_Nitrospiraceae	0.39%	1.19%	0.25%	5.07%	4.65%	12.81%	0.18%	3.82%	0.03%	2.10%	3.05%
Archaea;_Thaumarchaeota;_Marine_Group_I;_o;_f	0.99%	0.23%	0.00%	0.09%	0.01%	0.98%	0.00%	0.44%	0.00%	0.04%	0.28%
Bacteria;_Chlorobi;_Ignavibacteria;_Ignavibacteriales;Other	6.72%	34.25%	3.67%	5.38%	12.95%	2.23%	0.37%	11.85%	4.49%	1.66%	8.36%
Bacteria;_Proteobacteria;_Deltaproteobacteria;_Bdellovibrionales;_Bacteriovoracaceae	2.29%	0.97%	0.21%	4.31%	0.21%	11.38%	0.14%	4.21%	0.08%	3.75%	2.76%
Bacteria;_Candidate_division_OP11;_c;_o;_f	0.15%	1.73%	0.14%	0.46%	2.09%	0.42%	6.34%	0.25%	11.03%	0.06%	2.27%
Bacteria;_Bacteroidetes;_Sphingobacteriia;_Sphingobacteriales;_env.OPS_17	4.20%	3.28%	0.25%	7.09%	0.14%	0.68%	1.24%	3.85%	1.14%	0.64%	2.25%
Bacteria;_Proteobacteria;_Gammaproteobacteria;_Enterobacteriales;_Enterobacteriaceae	3.44%	1.01%	3.49%	1.16%	0.69%	1.47%	4.18%	0.39%	2.19%	0.53%	1.86%
Bacteria;_Proteobacteria;_Deltaproteobacteria;_Desulfuromonadales;_Geobacteraceae	0.02%	0.79%	0.00%	0.03%	0.14%	0.03%	0.05%	0.06%	0.00%	0.14%	0.13%
Bacteria;_Cyanobacteria;_ML635J-21;_o;_f	0.03%	0.06%	0.02%	0.06%	0.00%	0.34%	0.00%	0.02%	0.00%	0.23%	0.08%
Bacteria;_Cyanobacteria;_SHA-109;_o;_f	0.00%	0.00%	0.10%	0.00%	0.90%	0.00%	0.00%	0.00%	0.00%	0.00%	0.10%

Table 3: Relative abundance of taxa to the Family level. Overall 10 most abundant taxa listed, as well as other taxa of interest mentioned in the text and SI, ordered by relative abundance averaged across all samples. Taxa color coded by putative metabolism: red for aerobic iron oxidizers, purple for anoxygenic phototrophs, green for oxygenic phototrophs, blue for nitrifiers, and yellow for taxa with members performing a diverse range of metabolisms that can't be resolved with taxonomic resolution of available data.

References:

1. Bekker, A. et al. Iron Formations: Their Origins and Implications for Ancient Seawater Chemistry. Treatise on Geochemistry: Second Edition 9, (2013).
2. Beukes, N. J. "Sedimentology of the Kuruman and Griquatown iron-formations, Transvaal Supergroup, Griqualand West, South Africa."Precambrian Research 24.1 (1984): 47-84.
3. Beukes NJ and Klein C (1990) Geochemistry and sedimentology of a facies transition— from microbanded to granular iron-formation—in the early Proterozoic Transvaal Supergroup, South Africa. Precambrian Research 47: 99–139.
4. Beukes, N.J., Klein, C., Kaufman, A.J., and Hayes, J.M., 1990, Carbonate petrography, kerogen distribution, and carbon and oxygen isotope variations in and early Proterozoic transition from limestone to iron forma- tion deposition, Transvaal Supergroup, South Africa: Economic Geology and the Bulletin of the Society of Economic Geologists, v. 85, p. 663–690.
5. Bird, L. J., Bonnefoy, V. & Newman, D. K. Bioenergetic challenges of microbial iron metabolisms. Trends Microbiol. 19, 330–340 (2011).
6. Blöthe, M., and E. E. Roden. 2009. Microbial iron redox cycling in a circumneutral-pH groundwater seep. Appl. Environ. Microbiol. 75:468-473.
7. Bosak, T. et al. Cyanobacterial diversity and activity in modern conical microbialites. Geobiology 10, 384–401 (2012).

8. Bryant DA, Liu Z. 2013. Green Bacteria: Insights into Green Bacterial Evolution through Genomic Analyses. In Genome Evolution of Photosynthetic Bacteria, pp. 99–150. Academic Press
9. Byrne-Bailey, K. G. et al. Completed genome sequence of the anaerobic iron-oxidizing bacterium Acidovorax ebreus strain TPSY. J. Bacteriol. 192, 1475–1476 (2010).
10. Cairns-Smith, A.G., 1978, Precambrian solution photochemistry, inverse segregation, and banded iron formation: Nature, v. 276, p. 807–808.
11. Canfield, D. E. "A new model for Proterozoic ocean chemistry." Nature396.6710 (1998): 450-453.
12. Caporaso, J. G. et al. Ultra-high-throughput microbial community analysis on the Illumina HiSeq and MiSeq platforms. ISME J 6, 1621–1624 (2012).
13. Caporaso, J. Gregory, et al. "QIIME allows analysis of high-throughput community sequencing data." Nature methods 7.5 (2010): 335-336.
14. Chan, C., Emerson, D. & Luther, G. W. The role of microaerophilic Fe-oxidizing microorganisms in producing banded iron formations. Geobiology (2016).
15. CLOUD P. 1973. Paleoecological significance of the banded iron-formation. Economic Geology 68, 1135– 43.
16. Crossey, Laura J., et al. "Continental smokers couple mantle degassing and distinctive microbiology within continents." *Earth and Planetary Science Letters* 435 (2016): 22-30.

17. Crowe, S. A. et al. Photoferrotrophs thrive in an Archean Ocean analogue. Proc. Natl. Acad. Sci. 105, 15938–15943 (2008).

18. Davenport C, Ussery DW, Tümmler B. 2010. Comparative genomics of green sulfur bacteria. Photosynth. Res. 104(2-3):137–52

19. DeLong, Edward F., et al. The Prokaryotes: Alphaproteobacteria and Betaproteobacteria. Ed. Eugene Rosenberg. Berlin, Heidelberg: Springer Berlin Heidelberg, 2014.

20. Di Rienzi SC, Sharon I, Wrighton KC, Koren O, Hug LA, et al. 2013. The human gut and groundwater harbor non-photosynthetic bacteria belonging to a new candidate phylum sibling to Cyanobacteria. eLife. 2:e01102

21. Drever, James I. "Geochemical model for the origin of Precambrian banded iron formations." Geological Society of America Bulletin 85.7 (1974): 1099-1106.

22. Edgar RC. 2010. Search and clustering orders of magnitude faster than BLAST. Bioinformatics 26(19):2460-2461.

23. Ehrenreich, A., and Widdel, F., 1994, Anaerobic oxidation of ferrous iron by purple bacteria, a new type of phototrophic metabolism: Applied and Environmental Microbiology, v. 60, p. 4517–4526

24. Emerson, D. & Moyer, C. Isolation and characterization of novel iron-oxidizing bacteria that grow at circumneutral pH. Appl. Environ. Microbiol. 63, 4784–4792 (1997).Emerson, D. et al. A novel lineage of proteobacteria involved in formation of marine Fe-oxidizing microbial mat communities. PLoS One 2, (2007).

25. Emerson, D., Fleming, E. J. & McBeth, J. M. Iron-oxidizing bacteria: an environmental and genomic perspective. Annu. Rev. Microbiol. 64, 561–583 (2010).

26. Emerson, D. *et al*. Comparative genomics of freshwater Fe-oxidizing bacteria : implications for physiology , ecology , and systematics. *Front. Microbiol*. **4,** 1–17 (2013).

27. Emerson, Joanne B., et al. "Metagenomic analysis of a high carbon dioxide subsurface microbial community populated by chemolithoautotrophs and bacteria and archaea from candidate phyla." *Environmental microbiology* 18.6 (2016): 1686-1703.

28. España, Javier Sánchez, Esther Santofimia Pastor, and Enrique López Pamo. "Iron terraces in acid mine drainage systems: a discussion about the organic and inorganic factors involved in their formation through observations from the Tintillo acidic river (Riotinto mine, Huelva, Spain)." *Geosphere* 3.3 (2007): 133-151.

29. Fernández-Remolar, David C., and Andrew H. Knoll. "Fossilization potential of iron-bearing minerals in acidic environments of Rio Tinto, Spain: Implications for Mars exploration." Icarus 194.1 (2008): 72-85.

30. Finneran, K. T., Johnsen, C. V. & Lovley, D. R. Rhodoferax ferrireducens sp. nov., a psychrotolerant, facultatively anaerobic bacterium that oxidizes acetate with the reduction of Fe(III). Int. J. Syst. Evol. Microbiol. 53, 669–673 (2003).

31. Fischer, W. W. & Knoll, A. H. An iron shuttle for deepwater silica in late Archean and early Paleoproterozoic iron formation. Bull. Geol. Soc. Am. 121, 222–235 (2009).

32. Fischer, W. W. *et al*. SQUID-SIMS is a useful approach to uncover primary signals in the Archean sulfur cycle. *Proc. Natl. Acad. Sci. U. S. A.* **111,** 5468–73 (2014).

33. Fischer, W., Hemp, J. & Johnson, J. E. Evolution of Oxygenic Photosynthesis. Annu. Rev. Earth Planet. Sci. 44, (2016).

34. Fleming, E. J. *et al*. Hidden in plain sight : discovery of sheath-forming ,. *FEMS Micobiol Ecol* **85,** 116–127 (2013).

35. Fortney, N. W. et al. Microbial Fe(III) oxide reduction potential in Chocolate Pots hot spring, Yellowstone National Park. Geobiology (2016).

36. Fouke, Bruce W. "Hot-spring Systems Geobiology: abiotic and biotic influences on travertine formation at Mammoth Hot Springs, Yellowstone National Park, USA." *Sedimentology* 58.1 (2011): 170-219.

37. Francois, L.M., 1986, Extensive deposition of banded iron formations was possible without photosynthesis: Nature, v. 320, p. 352–354.

38. Geological Survey of Japan, AIST (ed.). 2012. Seamless digital geological map of Japan 1: 200,000. Jul 3, 2012 version. Research Information Database DB084, Geological Survey of Japan, National Institute of Advanced Industrial Science and Technology.

39. GOOD, I.J., 1953, The population frequencies of species and the estimation of population parameters: Biometrika, v. 40, p. 237–264.

40. Harder, E.C., 1919, Iron-Depositing Bacteria and Their Geologic Relations: U.S. Geological Survey Professional Paper 113, 89 p.

41. Hegler, Florian, et al. "Influence of seasonal and geochemical changes on the geomicrobiology of an iron carbonate mineral water spring." *Applied and environmental microbiology* 78.20 (2012): 7185-7196.

42. Heising, S., Richter, L., Ludwig, W. & Schink, B. Chlorobium ferrooxidans sp. nov., a phototrophic green sulfur bacterium that oxidizes ferrous iron in coculture with a 'Geospirillum' sp. strain. Arch. Microbiol. 172, 116–124 (1999).

43. Hemp J, Ward LM, Pace LA, Fischer WW. 2015a. Draft genome sequence of Levilinea saccharolytica KIBI-1, a member of the Chloroflexi class Anaerolineae. Genome Announc 3(6):e01357-15.

44. Hemp J, Ward LM, Pace LA, Fischer WW. 2015b. Draft genome sequence of Ardenticatena maritima 110S, a thermophilic nitrate- and iron-reducing member of the Chloroflexi class Ardenticatenia. Genome Announc 3(6):e01347-15.

45. HILL, M.O., 1973, Diversity and evenness: a unifying notation and its consequences: Ecology, v. 54, p. 427–432.

46. Hoffman, P. F., Kaufman, A., Halverson, G. & Schrag, D. A Neoproterozoic Snowball Earth. Science 281, 1342–1346 (1998).

47. Holland, Heinrich D. "The oceans; a possible source of iron in iron-formations." Economic Geology 68.7 (1973): 1169-1172.

48. Holland HD (1984) The chemical evolution of the atmosphere and oceans. Princeton University Press

49. Iino T, Mori K, Uchino Y, Nakagawa T, Harayama S, Suzuki K-I. 2010. Ignavibacterium album gen. nov., sp. nov., a moderately thermophilic anaerobic bacterium isolated from microbial mats at a terrestrial hot spring and proposal of Ignavibacteria classis nov., for a novel lineage at the periphery of green sulfur bacteria. Int. J. Syst. Evol. Microbiol. 60(Pt 6):1376–82

50. Johnson, Clark M., et al. "Iron isotopes constrain biologic and abiologic processes in banded iron formation genesis." *Geochimica et Cosmochimica Acta* 72.1 (2008): 151-169.

51. Johnson, J. E. et al. Manganese-oxidizing photosynthesis before the rise of cyanobacteria. Proc. Natl. Acad. Sci. 110, 11238–11243 (2013a).

52. Johnson, J. E. et al. Reply to Jones and Crowe: Correcting mistaken views of sedimentary geology, Mn-oxidation rates, and molecular clocks. Proc. Natl. Acad. Sci. 110, E4119–E4120 (2013b).

53. Kadnikov, Vitaly V., et al. "Genomic analysis of Melioribacter roseus, facultatively anaerobic organotrophic bacterium representing a novel deep lineage within Bacteriodetes/Chlorobi group." *PLoS One* 8.1 (2013): e53047.

54. Kappler, A. & Newman, D. K. Formation of Fe(III)-minerals by Fe(II)-oxidizing photoautotrophic bacteria. Geochim. Cosmochim. Acta 68, 1217–1226 (2004).

55. Kappler, A., Pasquero, C., Konhauser, K. O. & Newman, D. K. Deposition of banded iron formations by anoxygenic phototrophic Fe(II)-oxidizing bacteria. Geology 33, 864–865 (2005).

56. KASAMA T. & MURAKAMI T. 2001. The effect of micro- organisms on Fe precipitation rate at neutral pH. Chemical Geology 180, 117–28.

57. Katoh, Kazutaka, et al. "MAFFT: a novel method for rapid multiple sequence alignment based on fast Fourier transform." Nucleic acids research 30.14 (2002): 3059-3066.

58. Kirschvink, J. L. Late Proterozoic low-latitude global glaciation: the snowball Earth. In The Proterozoic Biosphere 52, 51–52 (1992).

59. Kiss, H. et al. Complete genome sequence of the filamentous gliding predatory bacterium Herpetosiphon aurantiacus type strain (114-95T). Stand. Genomic Sci. 5, 356–370 (2011).

60. Klatt, C. G. et al. Community ecology of hot spring cyanobacterial mats: predominant populations and their functional potential. ISME J. 5, 1262–1278 (2011).

61. Klein, C. Some Precambrian banded iron-formations (BIFs) from around the world: Their age, geologic setting, mineralogy, metamorphism, geochemistry, and origin. Am. Mineral. 90, 1473–1499 (2005).

62. Klueglein, N., and A. Kappler. "Abiotic oxidation of Fe (II) by reactive nitrogen species in cultures of the nitrate-reducing Fe (II) oxidizer Acidovorax sp.

BoFeN1–questioning the existence of enzymatic Fe (II) oxidation."Geobiology 11.2 (2013): 180-190.

63. Konhauser, K. O. et al. Could bacteria have formed the Precambrian banded iron formations? Geology 30, 1079–1082 (2002).
64. Konhauser, K. O., Newman, D. K. & Kappler, A. The potential significance of microbial Fe (III) reduction during deposition of Precambrian banded iron formations. Geobiology 3, 167–177 (2005).
65. Kopf, S. H., Henny, C. & Newman, D. K. Ligand-enhanced abiotic iron oxidation and the effects of chemical versus biological iron cycling in anoxic environments. Environ. Sci. Technol. 47, 2602–2611 (2013).
66. Kucera, S. & Wolfe, R. S. A Selective Enrichment Method for Gallionella Ferruginea. J. Bacteriol. 74, 344–349 (1957).
67. Ley, Ruth E., et al. "Obesity alters gut microbial ecology." Proceedings of the National Academy of Sciences of the United States of America 102.31 (2005): 11070-11075.
68. Li, Yi-Liang, et al. "Experimental low-grade alteration of biogenic magnetite indicates microbial involvement in generation of banded iron formations." *Earth and Planetary Science Letters* 361 (2013): 229-237.
69. Liu Z, Frigaard N-U, Vogl K, Iino T, Ohkuma M, et al. 2012a. Complete Genome of Ignavibacterium album, a Metabolically Versatile, Flagellated, Facultative Anaerobe from the Phylum Chlorobi. Front. Microbiol. 3:185

70. Liu Z, Klatt CG, Ludwig M, Rusch DB, Jensen SI, et al. 2012b. “Candidatus Thermochlorobacter aerophilum:” an aerobic chlorophotoheterotrophic member of the phylum Chlorobi defined by metagenomics and metatranscriptomics. ISME J. 6(10):1869–82

71. Mori, J. F. *et al*. Iron encrustations on filamentous algae colonized by Gallionella-related bacteria in a metal-polluted freshwater stream. *Biogeosciences* **12,** 5277–5289 (2015).

72. Morris, R. C. "A textural and mineralogical study of the relationship of iron ore to banded iron-formation in the Hamersley iron province of Western Australia." Economic Geology 75.2 (1980): 184-209.

73. Neubauer, S. C. et al. Life at the energetic edge: kinetics of circumneutral Fe oxidation by lithotrophic iron oxidizing bacteria isolated from the wetland plant rhizosphere. Appl. Environ. Microbiol. 68, 3988–3995 (2002).

74. Nunoura, Takuro, et al. "Isolation and characterization of a thermophilic, obligately anaerobic and heterotrophic marine Chloroflexi bacterium from a Chloroflexi-dominated microbial community associated with a Japanese shallow hydrothermal system, and proposal for Thermomarinilinea lacunofontalis gen. nov., sp. nov." *Microbes and Environments* 28.2 (2013): 228-235.

75. Oksanen, Jari, F. Guillaume Blanchet, Roeland Kindt, Pierre Legendre, Peter R. Minchin, R. B. O'Hara, Gavin L. Simpson, Peter Solymos, M. Henry H. Stevens and Helene Wagner (2016). vegan: Community Ecology Package. R package version 2.3-5. https://CRAN.R-project.org/package=vegan

76. Overmann J. 2008. Green nonsulfur bacteria. In Encyclopedia of Life Sciences (ELS). John Wiley & Sons, Chichester, United Kingdom.

77. Overmann, Jörg, and Ferran Garcia-Pichel. "The phototrophic way of life." The Prokaryotes. Springer Berlin Heidelberg, 2013. 203-257.

78. Pace LA, Hemp J, Ward LM, Fischer WW. 2015. Draft genome of Thermanaerothrix daxensis GNS-1, a thermophilic facultative anaerobe from the Chloroflexi class Anaerolineae. Genome Announc 3(6):e01354-15.

79. PARADA, A., NEEDHAM, D.M., AND FUHRMAN, J.A., 2015, Every base matters: assessing small subunit rRNA primers for marine microbiomes with mock communities, time-series and global field samples: Environmental Microbiology, v. 18, p. 1403–1414.

80. PARENTEAU, M. N. & CADY, S. L. Microbial Biosignatures in Iron-Mineralized Phototrophic Mats At Chocolate Pots Hot Springs, Yellowstone National Park, United States. *Palaios* **25,** 97–111 (2010).

81. Pierson, B. K., Parenteau, M. N. & Griffin, B. M. Phototrophs in high-iron-concentration microbial mats: Physiological ecology of phototrophs in an iron-depositing hot spring. Appl. Environ. Microbiol. 65, 5474–5483 (1999).

82. Pierson, B. K. & Parenteau, M. N. Phototrophs in high iron microbial mats: Microstructure of mats in iron-depositing hot springs. FEMS Microbiol. Ecol. 32, 181–196 (2000).

83. Podosokorskaya OA, Kadnikov VV, Gavrilov SN, Mardanov AV, Merkel AY, et al. 2012. Characterization of Melioribacter roseus gen. nov., sp. nov., a novel

facultatively anaerobic thermophilic cellulolytic bacterium from the class Ignavibacteria, and a proposal of a novel bacterial phylum Ignavibacteriae. Environ. Microbiol.

84. Podosokorskaya, Olga A., et al. "Ornatilinea apprima gen. nov., sp. nov., a cellulolytic representative of the class Anaerolineae." *International journal of systematic and evolutionary microbiology* 63.1 (2013): 86-92.
85. Posth, N. R., Konhauser, K. O. & Kappler, A. Microbiological processes in banded iron formation deposition. Sedimentology 60, 1733–1754 (2013).
86. Price MN, Dehal PS, Arkin AP. 2010. FastTree 2-Approximately Maximum-Likelihood Trees for Large Alignments. Plos One 5(3).
87. Quast, Christian, et al. "The SILVA ribosomal RNA gene database project: improved data processing and web-based tools." Nucleic acids research41.D1 (2013): D590-D596.
88. R Core Team. 2014. R: A language and environment for statistical computing. R Foundation for Statistical Computing, Vienna, Austria.
89. Rantamäki, S. et al. Oxygen produced by cyanobacteria in simulated Archaean conditions partly oxidizes ferrous iron but mostly escapes—conclusions about early evolution. Photosynth. Res. 1–9 (2016).
90. Rasmussen, B., Meier, D. B., Krapež, B. & Muhling, J. R. Iron silicate microgranules as precursor sediments to 2.5-billion-yearold banded iron formations. Geology 41, 435–438 (2013).

91. Rasmussen, B., Krapež, B., Muhling, J. R. & Suvorova, A. Precipitation of iron silicate nanoparticles in early Precambrian oceans marks Earth's first iron age. Geology 43, 303–306 (2015).

92. Rasmussen, B., Muhling, J. R., Suvorova, A. & Krapež, B. Dust to dust: Evidence for the formation of 'primary' hematite dust in banded iron formations via oxidation of iron silicate nanoparticles. Precambrian Res. 284, 49–63 (2016).

93. Roden, E., J. M. McBeth, M. Blothe, E. M. Percak-Dennett, E. J. Fleming, R. R. Holyoke et al. 2012. The microbial ferrous wheel in a neutral pH groundwater seep. Front. Microbiol. 3:172.

94. Roeselers, G. et al. Diversity of phototrophic bacteria in microbial mats from Arctic hot springs (Greenland). Environ. Microbiol. 9, 26–38 (2007).

95. Sekiguchi, Y. et al. Anaerolinea thermophila gen. nov., sp. nov. and Caldilinea aerophila gen. nov., sp. nov., novel filamentous thermophiles that represent a previously uncultured lineage of the domain Bacteria at the subphylum level. Int. J. Syst. Evol. Microbiol. 53, 1843–1851 (2003).

96. Shannon, C. E. (1948) A mathematical theory of communication. The Bell System Technical Journal, 27, 379–423 and 623–656.

97. Shih, P., Hemp, J., Ward, L., Matzke, N. & Fischer, W. 2016. Crown group oxyphotobacteria postdate the rise of oxygen. Geobiology.

98. SHIMAZU M., YAMADA K., NARITA E. & IGARASHI T. 1965. Geology of the Ainai-Kosaka-Oyu areas, Akita Prefecture. Bulletin of the Geological Survey of Japan 16, 22–30

99. SIMPSON, E.H., 1949, Measurement of diversity: Nature, v. 163, p. 688.

100. Singer, P. C. & Stumm, W. Acid Mine Drainage: The Rate-Determining Step. *Science (80-.).* **167,** 1121–1123 (1970).

101. Soo RM, Skennerton CT, Sekiguchi Y, Imelfort M, Paech SJ, et al. 2014. An expanded genomic representation of the phylum cyanobacteria. Genome Biol. Evol. 6(5):1031–45

102. Soo RM, Woodcroft BJ, Parks DH, Tyson GW, Hugenholtz P. 2015. Back from the dead; the curious tale of the predatory cyanobacterium Vampirovibrio chlorellavorus. PeerJ. 3:e968

103. Soo, Rochelle M., et al. "On the origins of oxygenic photosynthesis and aerobic respiration in Cyanobacteria." *Science* 355.6332 (2017): 1436-1440.

104. Stamps BW, Corsetti FA, Spear JR, Stevenson BS. 2014. Draft Genome of a Novel Chlorobi Member Assembled by Tetranucleotide Binning of a Hot Spring Metagenome. Genome Announc. 2(5):e00897–14 – e00897–14

105. Stookey, Lawrence L. "Ferrozine---a new spectrophotometric reagent for iron." Analytical chemistry 42.7 (1970): 779-781.

106. Stumm, W. & Lee, F. G. Oxygenation of ferrous iron. *Ind. Eng. Chem.* **53,** 143–146 (1961).

107. Swanner, E. D. et al. Modulation of oxygen production in Archaean oceans by episodes of Fe(II) toxicity. Nat. Geosci. 8, 126–130 (2015).

108. Takashima, C., Okumura, T., Nishida, S., Koike, H. & Kano, A. Bacterial symbiosis forming laminated iron-rich deposits in Okuoku-hachikurou hot spring, Akita Prefecture, Japan. Isl. Arc 20, 294–304 (2011).

109. Tosca, Nicholas J., Stephen Guggenheim, and Peir K. Pufahl. "An authigenic origin for Precambrian greenalite: Implications for iron formation and the chemistry of ancient seawater." Geological Society of America Bulletin 128.3-4 (2016): 511-530.

110. Trembath-Reichert E, Ward LM, Slotznick SP, Bachtel SL, Kerans C, Grotzinger JP, Fischer WW (2016) Gene sequencing microbial community analysis of mat morphologies, Caicos Platform, British West Indies, Journal of Sedimentary Research, in press.

111. Trouwborst, R. E., Johnston, A., Koch, G., Luther, G. W. & Pierson, B. K. Biogeochemistry of Fe(II) oxidation in a photosynthetic microbial mat: Implications for Precambrian Fe(II) oxidation. Geochim. Cosmochim. Acta 71, 4629–4643 (2007).

112. van Veen, W. L., Mulder, E. G. & Deinema, M. H. The Sphaerotilus-Leptothrix group of bacteria. Microbiol. Rev. 42, 329–356 (1978).

113. Wang Q, Garrity GM, Tiedje JM, Cole JR. 2007. Naive Bayesian classifier for rapid assignment of rRNA sequences into the new bacterial taxonomy. Appl Environ Microb 73(16): 5261-5267.

114. Ward, L. M., Kirschvink, J. L. & Fischer, W. W. 2016. Timescales of Oxygenation Following the Evolution of Oxygenic Photosynthesis. Orig. Life Evol. Biosph. 46(1) pp51-65.

115. Ward LM, Hemp J, Pace LA, Fischer WW. 2015a. Draft genome sequence of Leptolinea tardivitalis YMTK-2, a mesophilic anaerobe from the Chloroflexi class Anaerolineae. Genome Announc 3(6):e01356-15.

116. Ward LM, Hemp J, Pace LA, Fischer WW. 2015b. Draft genome sequence of Herpetosiphon geysericola GC-42, a nonphototrophic member of the Chloroflexi class Chloroflexia. Genome Announc 3(6):e01352-15

117. Wickham, H. ggplot2: Elegant Graphics for Data Analysis. Springer-Verlag New York, 2009.

118. Widdel, F., Schnell, S., Heising, S., Ehrenreich, A., Assmus, B., and Schink, B., 1993, Ferrous iron oxidation by anoxygenic phototrophic bacteria: Nature, v. 362, p. 834–836.

119. Yamada T, Sekiguchi Y, Hanada S, Imachi H, Ohashi A, Harada H,Kamagata Y. 2006. Anaerolinea thermolimosa sp. nov., Levilinea saccharolyticagen. nov., sp. nov. and Leptolinea tardivitalis gen. nov., sp. nov., novel filamentous anaerobes, and description of the new classes Anaerolineae classis nov.and Caldilineae classis nov. in the bacterial phylum Chloroflexi. Int J Syst Evol Microbiol 56:1331–1340.

120. Yamada, T. & Sekiguchi, Y. Cultivation of uncultured chloroflexi subphyla: significance and ecophysiology of formerly uncultured chloroflexi ‘subphylum i’

with natural and biotechnological relevance. Microbes Environ. 24, 205–216 (2009).

Supplemental Information:

Materials and methods:

Rarefaction plots were produced using QIIME version 1.8.0 (Caporaso et al., 2010) (Supplemental Figure 1). We used the UniFrac distance metric (Lozupone and Knight 2005) to assess the microbial community phylogenetic similarity of microbial communities (Supplemental Table 1).

Light microscopy images (Supplementary Figure 2) were taken on a Zeiss Axio Imagers 2 Upright microscope (Zeiss, Germany) with 40x and 100x objective lens. Epi-fluorescent images of DAPI (4'6-diamidino-2-phenylindole)-stained samples were taken with an excitation wavelength below 395 nm and an emission wavelength between 420 and 470 nm. The autofluorescence of Cyanobacteria was detected by exposing the sample to a wavelength of between 395 and 440 nm and detecting the emission at a wavelength of 470 nm. Images of DAPI fluorescence and autofluorescence were overlain using the FIJI software package (http://pacific.mpi-cbg.de).

Secular and paleoenvironmental changes in the redox state of iron in iron formations:

BIF deposits are compositionally, texturally, and sedimentologically diverse and consequently may not have a single causal mechanism of origin (Fischer and Knoll 2009). Broadly, BIFs can be grouped into three categories based on age of deposition, each with characteristic mineralogical and redox compositions and hypothesized formation mechanisms: Archean (and early Paleoproterozoic) BIF, which formed before the GOE, middle to late Paleoproterozoic BIF, which formed after the GOE and before ~1.8 Ga, and

Neoproterozoic BIF, which formed later in time, principally ~0.8-0.6 Ga, associated with Cryogenian glacial intervals (Hoffman et al. 1998, Kirschvink 1992). Archean BIFs consist primarily of well-laminated, sediment-starved and often deep water facies, consistent with deposition in an anoxic environment where deep waters were enriched in Fe(II) and could be oxidized either biotically or abiotically during mixing into the photic zone. This style of BIF exists throughout Archean and early Paleoproterozoic successions until the GOE. The iron minerals that comprise this category of BIF are made up largely of iron carbonates and silicates (Beukes 1984, Beukes and Klein 1990, Bekker et al. 2013, Rasmussen et al. 2013, Rasmussen et al. 2015, Rasmussen et al. 2016). These BIFs contain a high proportion of reduced iron, reflecting some combination of primary deposition of ferrous minerals (Rasmussen et al. 2013, Rasmussen et al. 2015, Rasmussen et al. 2016) and deposition of iron oxides followed by early microbial re-reduction associated with respiration of organic carbon (Konhauser et al. 2005, Fischer and Knoll 2009, Fischer et al. 2009, Bontognali et al. 2013). The most abundant iron oxide phase in Archean BIFs is magnetite, which has a late diagenetic origin where it occurs (Han 1978, Beukes 1984, Beukes et al. 1990, Fischer and Knoll 2009). Paleoproterozoic BIFs range from ~2.3 Ga to 1.8 Ga, and commonly consist of more granular and oolitic facies with current-generated structures such as dune- and ripple-scale cross-stratification, reflecting deposition in relatively higher energy, shallower water environments. This is consistent with oxidation via atmospheric O_2 of iron sourced from anoxic basinal waters and pore fluids. Paleoproterozoic BIFs typically contain higher abundances of hematite, magnetite, and other ferric iron minerals than observed in Archean BIFs (Klein 2005, Fischer and Knoll 2009, Bekker et al. 2013),

consistent with deposition in a more oxidizing world where carbon remineralization is driven more by aerobic respiration than by iron reduction. Furthermore, Paleoproterozoic BIFs contain much lower organic carbon than Archean BIFs (Fischer et al. 2009), suggesting that organic matter remineralization was much more efficient, as would be expected for an aerobic respiration-driven system. BIFs largely disappear from middle Proterozoic basins, likely driven by the increased abundances of both oxygen and sulfur in the fluid Earth (Canfield 1998), until they reappear between ~750 and 635 Ma in association with Cryogenian glacial intervals (Kirschvink et al. 1992, Hoffman et al. 1998). Neoproterozoic BIFs are highly unique in that they are made up almost entirely by ferric iron minerals (primarily hematite) (Klein 2005).

Additional discussion of the microbiology at OHK:

Interestingly, the water and minerals at OHK contain a high proportion of Xanthomonadaceae. Members of the Xanthamonadaceae family within the Gammaproteobacteria are typically plant-associated bacteria, particularly pathogens (Starr 1981). The Xanthomonadaceae sequences present at OHK are most similar (95% identity) to *Thermomonas*, a genus that includes members such as *Thermomonas hydrothermalis* isolated from hot springs where they act as aerobic heterotrophs (Alves et al. 2003).

While concentrations of fixed nitrogen species at OHK were low (no detectable nitrate or nitrite, and a maximum of 0.37 mg/l ammonia in the source pool)(Table 1), sequences associated with diverse nitrogen cycling organisms were recovered (Table 3). These include members of the Nitrospiraceae at up to 12.8% in the Old Stream Mineral

sample. The Nitrospiraceae, including the genus *Nitrospira*, are typically characterized as nitrite oxidizers (Bock and Wagner 2006) but are also one of the first groups known to possess the capacity for complete nitrification (comammox) (Daims et al. 2015, van Kessel et al. 2015).

Members of the Marine Group 1 Thaumarchaeota were the most abundant archaeal taxon observed at OHK (up to ~1% in the Deep Source Mineral and Old Source Water samples)(Table 3). This group is commonly characterized by aerobic ammonia oxidation in open ocean environments (e.g. Spang et al. 2010, Swan et al. 2014). The ammonia-oxidizing archaea are typically adapted to much lower ammonia concentrations than ammonia oxidizing bacteria (Martens-Habbena et al. 2009, Hatzenpichler 2012), consistent with their presence at OHK where concentrations of fixed nitrogen are low.

Although we observed nitrifying organisms at OHK, their metabolic byproducts—nitrite and nitrate—were not detected (Table 1). This may reflect the rapid reaction of oxidized nitrogen species with ferrous iron, which can proceed either via biological or abiotic mechanisms (Straub et al. 1996, Klueglein and Kappler 2013, Kopf et al. 2013). Like with many cycles that contain reactive intermediates, the low standing stocks of fixed nitrogen species may not preclude its overall importance to biogeochemical cycling, and thus a component of iron oxidation at OHK may occur through a cryptic nitrogen cycle. Even if this is the case, the ultimate source of oxidizing potential would nonetheless originate in atmospheric O_2 used for nitrification. However, it is interesting to note that many known iron oxidizers are nested within nitrifying clades (e.g. *Gallionella* within Nitrosomonadales, *Leptospirillum* within Nitrospirae)—hinting at metabolic, ecological,

and evolutionary links between these chemoautotrophic metabolisms. This also leaves open the possibility that the Nitrospiraceae sequences observed here are associated not with nitrite oxidizers as is typically seen, but instead could represent a group of iron oxidizers within this clade.

Members of the Candidate Phylum OP11 are abundant at OHK, particularly in the Bubble Pool mineral fraction where they made up ~11% of sequence reads (Table 3). OP11, also known as Microgenomates, are a clade within the enigmatic Candidate Phyla Radiation of bacteria (Brown et al. 2015, Eloe-Fadrash et al. 2016, Hug et al. 2016). Though members of OP11 thus far remain uncultured, assembly and binning of metagenomic sequence data suggests that these organisms are anaerobes with a widespread capacity for fermentation-based metabolism (Wrighton et al. 2012).

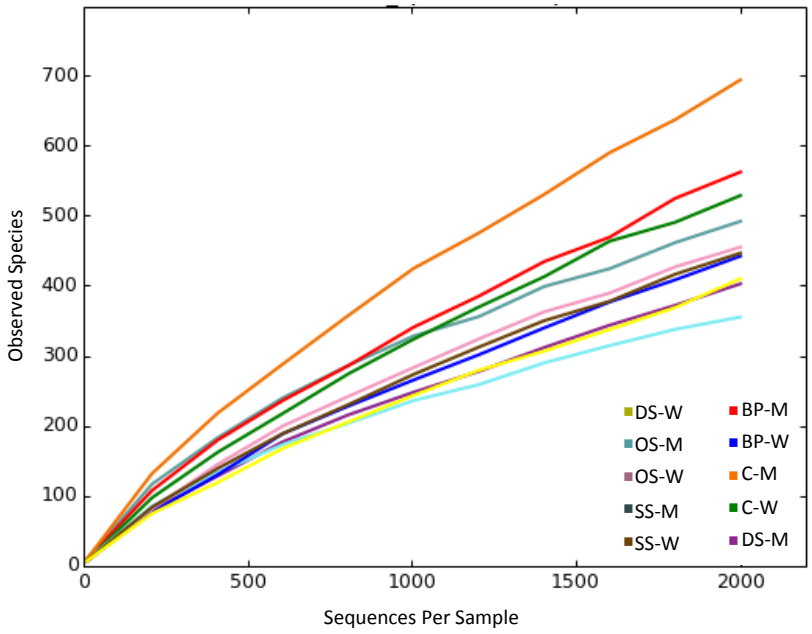

Supplemental Figure 1: Subsampling (rarefaction) diversity curves of OHK samples. Sampled to a depth of 2000 reads per sample. The microbial diversity at OHK is fairly well sampled, even at this low level of sampling depth, particularly near the source where diversity is lower overall. Downstream samples, particularly the Canal Mineral sample, are more diverse and additional sequencing depth would likely reveal additional diversity.

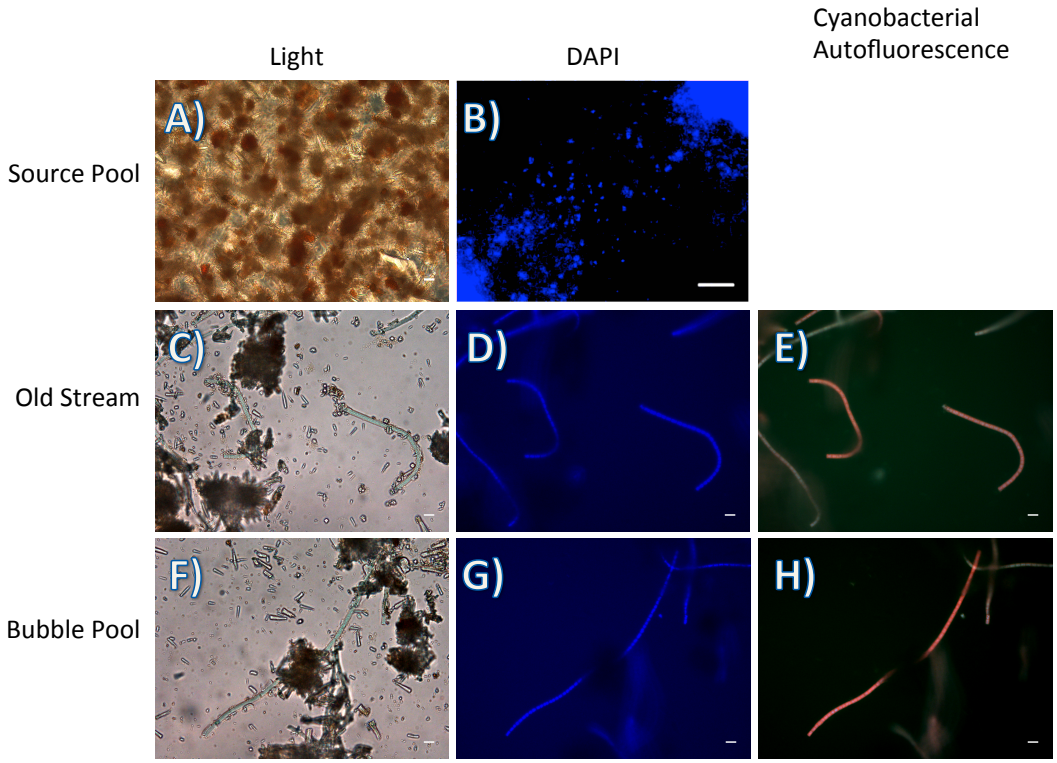

Supplemental Figure 2: Light and epifluorescence microscopy images of representative OHK hot spring samples. Top row (A&B): Source pool; middle row (C-E): Old Stream; bottom row (F-H): Bubble Pool; Left column: light microscopy showing mineral grains and associated microbial cells; middle column: fluorescence image of same samples, showing DAPI-stained cells in blue; right column: same samples showing cyanobacterial autofluorescence. Cyanobacterial filaments are apparent in Old Stream and Bubble Pool samples, but do not appear in Source Pool samples, consistent with molecular data. Scale bars are 10 μm.

	OS-W	C-W	SS-W	DS-M	BP-W	SS-M	DS-W	OS-M	BP-M	C-M
OS-W	0	0.2719	0.3201	0.2891	0.5340	0.5710	0.4676	0.3811	0.5826	0.6008
C-W		0	0.2197	0.2568	0.5317	0.5442	0.3974	0.3354	0.5685	0.6066
SS-W			0	0.3088	0.5247	0.6120	0.4710	0.4174	0.6473	0.6919
DS-M				0	0.5776	0.5463	0.3378	0.3659	0.5401	0.5582
BP-W					0	0.8317	0.7398	0.6608	0.8481	0.8715
SS-M						0	0.5862	0.5706	0.5464	0.5053
DS-W							0	0.4050	0.5578	0.5773
OS-M								0	0.5156	0.5568
BP-M									0	0.3697
C-M										0

Supplemental Table 1:

Weighted Unifrac matrix, showing the dissimilarity between samples, incorporating both differences in presence/absence as well as relative abundance of taxa (color coded to highlight relative dissimilarity—dark green is <0.33 dissimilarity, pale green >0.33 and <0.5, yellow >0.5 and <0.66, orange >0.66). Samples from the same location tend to be relatively similar, and water samples tend to be relatively similar. The Bubble Pool Water sample was most dissimilar to the other samples. OS, Old Stream; C, Canal; SS, Shallow Source Pool; DS, Deep Source Pool; BP, Bubble Pool; -W, filtered water sample; -M mineral precipitate sample.

Supplemental references:

1. Alves, Marta P., et al. "Thermomonas hydrothermalis sp. nov., a new slightly thermophilic γ-proteobacterium isolated from a hot spring in central Portugal." *Systematic and applied microbiology* 26.1 (2003): 70-75.
2. Bock, Eberhard, and Michael Wagner. "Oxidation of inorganic nitrogen compounds as an energy source." The prokaryotes. Springer New York, 2006. 457-495.

3. Bontognali, T. R. R., Fischer, W. W. & Föllmi, K. B. Siliciclastic associated banded iron formation from the 3.2Ga Moodies Group, Barberton Greenstone Belt, South Africa. Precambrian Res. 226, 116–124 (2013).
4. Brown, C. T. et al. Unusual biology across a group comprisingmore than 15% of domain Bacteria Christopher. Nature 523, 208–211 (2015).
5. Daims, Holger, et al. "Complete nitrification by Nitrospira bacteria." Nature528.7583 (2015): 504-509.
6. Eloe-Fadrosh, E. A., Ivanova, N. N., Woyke, T. & Kyrpides, N. C. Metagenomics uncovers gaps in amplicon-based detection of microbial diversity. Nat. Microbiol. 15032 (2016).
7. Fischer, W. W. et al. Isotopic constraints on the Late Archean carbon cycle from the Transvaal Supergroup along the western margin of the Kaapvaal Craton, South Africa. Precambrian Res. 169, 15–27 (2009).
8. Han, T.-M., 1978, Microstructures of magnetite as guides to its origin in some Precambrian iron-formations: Fortschritte der Mineralogie, v. 56, p. 105–142.
9. Hatzenpichler, R. Diversity, physiology, and niche differentiation of ammonia-oxidizing archaea. *Appl. Environ. Microbiol.* **78,** 7501–7510 (2012).
10. Hug, L. A. et al. A new view of the tree and life's diversity. Nat. Microbiol. (2016).
11. van Kessel, M. A. H. J. *et al*. Complete nitrification by a single microorganism. *Nature* **528,** 1–17 (2015).

12. LOZUPONE, C., AND KNIGHT, R., 2005, UniFrac: a new phylogenetic method for comparing microbial communities: Applied and Environmental Microbiology, v. 71, p. 8228–8235.

13. Martens-Habbena, W. et al. Ammonia oxidation kinetics determine niche separation of nitrifying Archaea and Bacteria. Nature 461, 976–979 (2009).

14. Spang, A. et al. Distinct gene set in two different lineages of ammonia-oxidizing archaea supports the phylum Thaumarchaeota. Trends Microbiol. 18, 331–340 (2010).

15. Starr, Mortimer P. "The genus Xanthomonas." The prokaryotes. Springer Berlin Heidelberg, 1981. 742-763.

16. Straub, Kristina Lotte, et al. "Anaerobic, nitrate-dependent microbial oxidation of ferrous iron." Applied and Environmental Microbiology 62.4 (1996): 1458-1460.

17. Swan, B. K. et al. Genomic and metabolic diversity of marine group i thaumarchaeota in the mesopelagic of two subtropical gyres. PLoS One 9, (2014).

18. Wrighton, K. et al. Fermentation, hydrogen, and sulfur metabolism in multiple uncultivated bacterial phyla. Science (80-.). 337, 1661–1666 (2012).